

LOCKHEED MARTIN ENERGY RESEARCH LIBRARIES



3 4456 0513636 8

CENTRAL RESEARCH LIBRARY

ORNL-TM-4672

cy 1

A SPECTROSCOPIC STUDY
IN THE VACUUM ULTRAVIOLET
OF A NEON PLASMA IN ELMO
(thesis)

J. A. Cobble

OAK RIDGE NATIONAL LABORATORY
CENTRAL RESEARCH LIBRARY
DOCUMENT COLLECTION

LIBRARY LOAN COPY

DO NOT TRANSFER TO ANOTHER PERSON

If you wish someone else to see this
document, send in name with document
and the library will arrange a loan.

UCN-7969
(3 3-67)



OAK RIDGE NATIONAL LABORATORY

OPERATED BY UNION CARBIDE CORPORATION • FOR THE U.S. ATOMIC ENERGY COMMISSION

Contract No. W-7405-eng-26

THERMONUCLEAR DIVISION

A SPECTROSCOPIC STUDY IN THE VACUUM ULTRAVIOLET
OF A NEON PLASMA IN ELMO

J. A. Cobble

SEPTEMBER 1974

Submitted as a thesis to the Graduate Council of the
University of Tennessee in partial fulfillment of the
requirements for the degree of Doctor of Philosophy.

OAK RIDGE NATIONAL LABORATORY
Oak Ridge, Tennessee 37830
operated by
UNION CARBIDE CORPORATION
for the
U. S. ATOMIC ENERGY COMMISSION



3 4456 0513636 8



ACKNOWLEDGMENTS

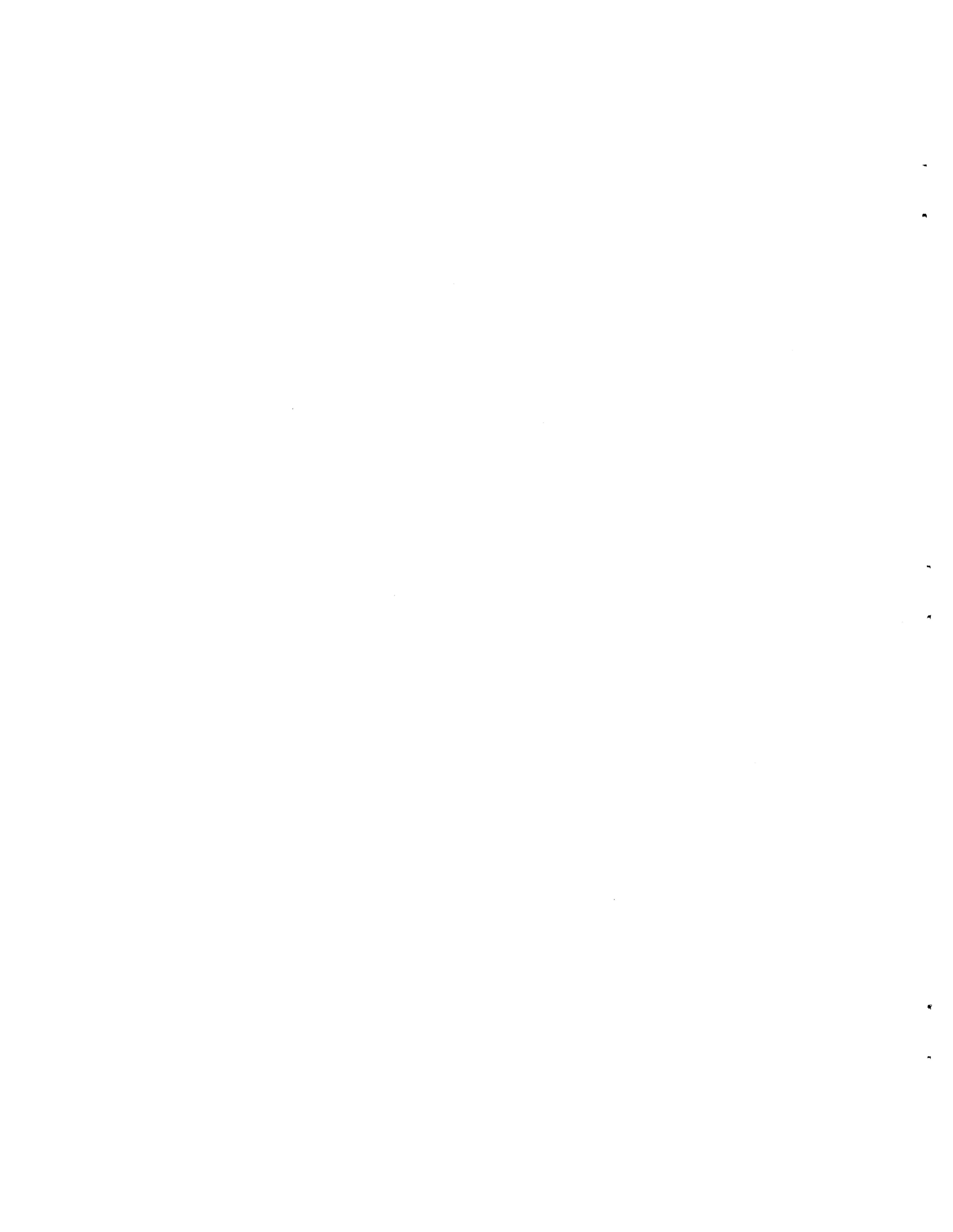
This research was sponsored by the U. S. Atomic Energy Commission under contract with the Union Carbide Corporation in the Thermonuclear Division of Oak Ridge National Laboratory. I express my thanks to Herman Postma and John Clarke who as directors of the Thermonuclear Division provided me the opportunity to do a dissertation there.

I give thanks to Granvil Kyker of Oak Ridge Associated Universities for the year and a half of financial support awarded me by that agency and to John Martin of the Physics Division of ORNL for the six months of stipends offered by that source.

I express gratitude to group leader Ray Dandl for recommending the subject of this thesis, for the tolerance he had for me within the ELMO group, and for letting me take part in the activities of that group.

My primary director and source of encouragement has been F. Robert Scott of the University of Tennessee and the AEC's Controlled Thermonuclear Research Program. I thank him for my introduction into the Thermonuclear Division and for sound advice concerning this report and things in general.

Others to whom acknowledgment is due include J. Rand McNally, Jr., and Hideo Ikegami for their suggestions and constructive criticism of various phases of the work. Thanks also go to the whole of the ELMO staff, especially Norma Bryson for typing the final manuscript.



ABSTRACT

ORNL's ELMO device contains an electron-cyclotron-heated plasma in a simple mirror trap. The relative intensities of line radiation in the vacuum ultraviolet for five charge states of neon in ELMO have been measured with a calibrated, grazing incidence spectrometer.

Theoretical models for the excitation and ionization of atomic systems in the plasma are based on an optically thin, corona approximation in which atom-electron collisions play the main part. The resulting population-balance equations for excited states in the excitation model are employed to measure the temperature of cold electrons which form the background plasma. Once this parameter is known, the density ratios of the various charge states present may be determined. Absolute densities of ions and electrons following from pressure measurements are next presented. Comparison of experimental results with the theoretical ionization model permits the estimation of a particle containment time and an ion temperature.

Calculated plasma parameters are consistent with previous measurements of these variables when such measurements exist, and there is qualitative agreement with the estimates when no other assessment is available.

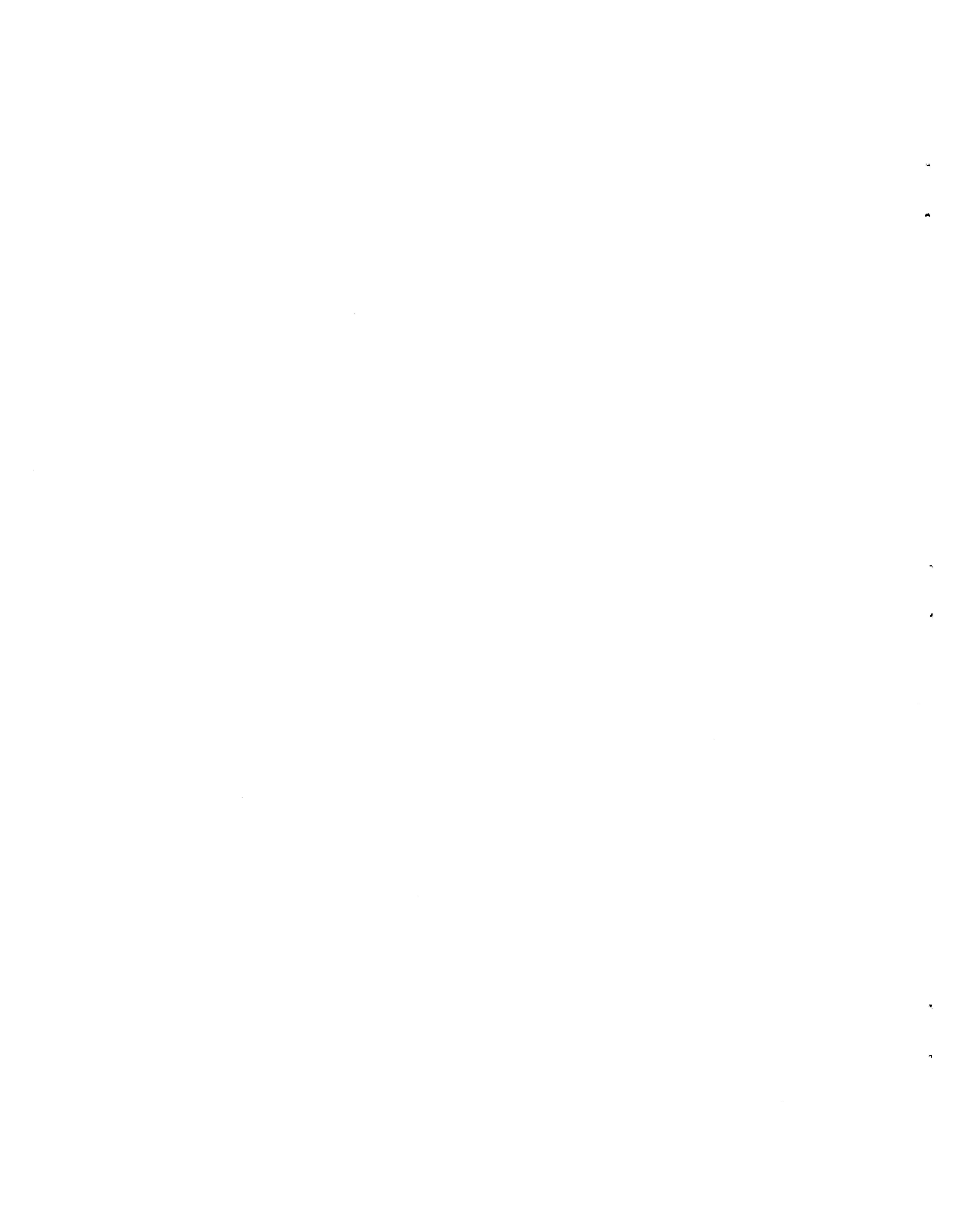


TABLE OF CONTENTS

SECTION	PAGE
I. INTRODUCTION	1
Plasmas and Plasma Physics	1
Plasma physics	1
Electrical neutrality and the Debye length	1
More on the definition of a plasma	3
Wave propagation and the plasma frequency	4
Magnetic Confinement of Plasmas	5
Motion of a charged particle in a magnetic field	5
Magnetic mirrors	6
Mirror confinement	7
ELMO	9
Spectroscopy as a Plasma Diagnostic	9
Plasma spectroscopy	11
Plasma model	12
An Outline of the Dissertation	12
II. A REVIEW OF ELMO PLASMA PARAMETERS	14
Experimental Variables	14
Pressure	14
Magnetic field	16
Microwave power	16
Intrinsic Variables	19
The electron plasma	19
The ion plasma	21

SECTION	PAGE
III. THE PLASMA MODEL: THE LINK BETWEEN THEORY	
AND EXPERIMENT	24
The Excitation Model	24
Common plasma models	24
Methods for populating excited states	27
Model simplification	27
The electron-impact model	36
Population balance equations	38
A Derivation of Intrinsic Parameters from the	
Excitation Model	39
The cold-electron temperature	39
The densities of the charge states	40
The electron density	41
The Ionization Model	42
Methods of ionization and model reduction	42
Electron-impact ionization modes	43
The ion population equations	48
Plasma Information from the Ionization Model	50
Ion containment and temperature	50
The role of the hot electrons	51
IV. EXPERIMENTAL CONSIDERATIONS	52
The Vacuum Ultraviolet Spectrometer	52
Description	52
Mounting	55

SECTION	PAGE
The Detector	57
Description of the CEM	57
Circuitry	58
Calibration	60
Wavelength calibration	60
Intensity calibration	60
Output	66
Signal amplitude	66
Dispersion and resolution	68
V. OBSERVATIONS AND MEASUREMENTS	70
General Observations	70
Line identification	70
Impurities	71
Charge states	72
The neon data	72
Observations on cascade feeding and resonance self-absorption	73
The Cold-Electron Temperature	76
The hot to cold electron density ratio	76
Determination of the cold-electron temperature	78
Densities of Plasma Charge States	78
Ion density calculations	79
Electron density calculations	81

SECTION	PAGE
Determination of Containment Time and Ion	
Temperature	82
Particle containment	82
Ion heating	86
Error Analysis	86
Experimental errors	86
Theoretical errors	87
The effect on calculated parameters	90
VI. CONCLUSION	91
Comparison of Measurements	91
Electron parameters	91
Ion parameters	91
The Success of the Theoretical Model	92
Possible Applications	93
High-Z ion sources	93
Impurity radiation	93
Excitation and ionization rates	94
Suggestions for Future Work	94
LIST OF REFERENCES	97

LIST OF TABLES

TABLE	PAGE
1. Ionization Energies for Different Neon Ions	44
2. Charge Spectra Resulting from a K- or L-Shell Vacancy in Neutral Neon	47
3. Line Pairs Used in the Branching Ratio Calibration	62
4. Sensitivity Versus Wavelength for the Jarrell-Ash Visible Spectrometer	63
5. Average Ratios of Spectrometer Responses to Calibration Line Pairs	64
6. Relative Intensities of the Multiplet Components of Ne III 489 as Percentages of the Total Multiplet Strength	68
7. Relevant Neon Transitions with Wavelengths, Excitation Energies, Transition Probabilities, Oscillator Strengths, and Relative Intensities	74
8. Solutions for the Cold-Electron Temperature from the 55 Pairs of Ne III Lines (in eV)	79
9. Relative Ground-State Densities of Five Neon Charge States as Determined by Pairs of Spectral Lines	80
10. Fractional Populations and Densities of Neon Charge States for $n_T = 8.0 \times 10^{11} \text{ cm}^{-3}$	81
11. A Computer Printout for the Time Dependence of the Fractional Populations of the Neon Charge States.. . . .	84
12. The Ratio of Theoretical to Experimental F_k 's	85

LIST OF FIGURES

FIGURE	PAGE
1. A Cut-Away View of ELMO	10
2. ELMO Magnetic Field On Axis per 1000 Amperes Total Current versus Distance from One End of the Microwave Cavity	17
3. Mod-B Contours for ELMO System with Plasma Profile Derived from Diamagnetic Data	18
4. A Simplified Term Diagram of Ne I Showing the Cascade Feeding of the Strongest UV Transitions	30
5. A Simplified Term Diagram of Some UV Transitions in Ne II--Wavelengths in Angstroms	31
6. A Simplified Term Diagram of Some UV Transitions in Ne III--Wavelengths in Angstroms	32
7. A Simplified Term Diagram of Some UV Transitions in Ne IV--Wavelengths in Angstroms	33
8. A Simplified Term Diagram of Some UV Transitions in Ne V--Wavelengths in Angstroms	34
9. The Rowland Circle Spectrometer Configuration	53
10. A Block Diagram of the Detector System	59
11. Normalized Sensitivity of the XUV Spectrometer versus Wavelength--The Least Squares Fit to a Straight Line Omits the He I 537 Data Point	65
12. Strip Chart Trace of the Ne III 489 Multiplet	67
13. Theoretical Ratios of Excitation Rates of Ne III 379.3 and Ne III 488.1 for a Family of ϵ 's	77
14. The Theoretical Time Evolution of the F_k 's for $\epsilon = 0.06$	83

I. INTRODUCTION

A. PLASMAS AND PLASMA PHYSICS

Plasma Physics

The plasma state of matter may be thought of as a collection of atomic particles with enough energy that a considerable degree of ionization has occurred. The plasma is usually overall neutral electrically, and it is large enough that the collective effects of ions and electrons dominate over the effects of individual particles. (The term "ion" will denote a positively charged atom.) Atoms, if not completely stripped of electrons, are continually being excited to higher quantum states. Thus, they spontaneously emit their characteristic line radiation as they de-excite, or they undergo further ionization.

Examples of plasma are numerous.¹ Common earth-bound plasmas are fire, lightning, and the ionosphere. Solar wind and the sun itself are extraterrestrial instances. Ordinary fluorescent lights are man-made plasmas as are the objects of current research in the field of controlled thermonuclear fusion. Obviously, these examples vary widely in their physical properties. It is the science of plasma physics which endeavors to expose them.

Electrical Neutrality and the Debye Length

The concept of electrical neutrality mentioned in the first paragraph may be expanded as follows. At any particular time in a small volume surrounding a particle, there may be a majority of ions or electrons. If

a charge is assigned to the particle in question, the volume around it will tend to be filled by more oppositely-charged than like-charged particles on account of simple electrostatic forces. Averaged over time, then, ions will be surrounded by an "atmosphere" of net negative charge, and vice versa for electrons. Therefore, on a microscopic scale the charge density of a region of the plasma may be non-vanishing.² However, if a large volume of plasma is considered, the aggregation of all particles tends to have net charge equal to zero. If this is not so, the electrostatic potential builds up. Without special devices to maintain this potential, charged particles will respond so as to relax the force on them and restore electrical neutrality.³

The minimum volume over which neutrality may be expected to prevail is several times the radius of the miniature charged atmospheres introduced above. The radius of the negatively charged atmospheres around an ion is given by:

$$h = \left[\frac{T_e}{4\pi n_e e^2} \right]^{\frac{1}{2}}, \quad (I-1)$$

where T_e is the kinetic temperature of electrons in energy units, n_e the electron density, and e the charge of an electron. (CGS units will be used throughout unless otherwise specified.) By kinetic temperature is meant:

$$T_e = k_B T = \frac{2}{3} E, \quad (I-2)$$

where k_B is Boltzmann's constant and T is the temperature in degrees Kelvin. E is the mean energy (of electrons in this case). If the

negative charge in a region with dimensions $10 h$ deviates by one percent from the net positive charge content, the electrostatic potential energy per electron approaches E in magnitude.⁴ The distance, h , called the Debye length, is also a measure of the distance from an ion beyond which its negatively charged atmosphere screens its Coulomb field from other ions.⁵ Equation (I-1) may be written:

$$h = 2.35 \times 10^4 \left(T_e / n_e \right)^{\frac{1}{2}}, \quad (\text{I-3})$$

where T_e is given in keV. Thus, if $T_e \sim 10$ eV, for example, and $n_e \sim 3 \times 10^{11} \text{ cm}^{-3}$, then $h \sim 0.0043$ cm.

More on the Definition of a Plasma

The Debye length is now used to elaborate the definition of a plasma. To insure charge neutrality, the dimensions of the plasma must be many times the Debye length. The next consideration is the matter of collective effects. Some definitions are in order first. A short-range interaction is a Coulomb-scattering event between two particles in which the impact parameter, b , is sufficiently small that at least a 90° deflection of the incoming test particle is achieved. A long-range interaction is the same except that b is not small enough for a 90° scatter. If the number of charged particles in a sphere of radius h is large, the effects of long-range interactions are dominant over those of short range.⁶ The reason for this is that the number of long-range encounters is very large. For the plasma cited before ($T_e \sim 10$ eV, $n_e \sim 3 \times 10^{11} \text{ cm}^{-3}$), there are nearly 10^5 electrons in the so-called Debye sphere. What this means is that the behavior of the plasma is dictated not by

what happens to or on account of single particles but by the collective motion of large numbers of particles.

Wave Propagation and the Plasma Frequency

Suppose an electromagnetic wave is incident on the plasma. Charges near the surface will react to exclude the wave from the plasma interior. If the wave frequency is too high, they will not be able to screen the wave from the bulk of the plasma, and it will propagate. If, however, the charges can rearrange themselves quickly enough, i.e., if the frequency of the wave is below a certain value, the wave will not be transmitted.^{7,8} The critical value is the plasma frequency, ω_p , where

$$\omega_p = \left(\frac{4\pi n e^2}{m} \right)^{\frac{1}{2}} \quad (\text{I-4})$$

and m is the mass of the charges under consideration. For electrons

$$\omega_p = 5.64 \times 10^4 n_e^{\frac{1}{2}} \quad (\text{I-5})$$

Therefore, if $n_e \sim 3 \times 10^{11} \text{ cm}^{-3}$, $\omega_p \sim 3.1 \times 10^{10} \text{ sec}^{-1}$. To return to wave propagation, if ω is the angular frequency of the wave,

$$\omega > \omega_p \quad (\text{I-6})$$

implies transmission. Thus, in the $3 \times 10^{11} \text{ cm}^{-3}$ plasma, the approximate cut-off in wavelength is 6.1 cm, and all shorter wavelengths are propagated.

B. MAGNETIC CONFINEMENT OF PLASMAS

There are several ways by which plasmas are contained. A fluorescent light employs a glass tube to form the boundaries of its plasma. The sun uses gravitational confinement. Earth-bound plasmas of thermonuclear interest generally depend on magnetic fields to constrain the plasma because no solid wall material will withstand the 100 million degrees Kelvin necessary to ignite and operate a power-producing fusion reactor.⁹ Even the 10 eV plasma used as an example in the previous section has a temperature of over 100,000°K via Equation (I-2).

Motion of a Charged Particle in a Magnetic Field

The motion of a charged particle in a uniform, one-dimensional magnetic field, B , is well known.^{10,11} As the particle spirals around a field line at constant speed, its orbit traces out a helix. Its velocity, v_{\parallel} , parallel the field is constant; the perpendicular velocity, v_{\perp} , is related to the angular velocity, ω_c , by:

$$\omega_c = \frac{v_{\perp}}{r} = \frac{qB}{mc} \quad , \quad (I-7)$$

where r is the helical radius, q/m the particle's charge to mass ratio, and c the speed of light. The cyclotron frequency is a name often applied to ω_c . For an electron in a 15 kG (kilogauss) field, Equation (I-7) yields $\omega_c = 2.6 \times 10^{11} \text{ sec}^{-1}$ or about 42 gigahertz.

Another useful quantity for particles in a magnetic field is the magnetic moment, μ , where if E_{\perp} is the energy perpendicular to B ,

$$\mu = \frac{E_{\perp}}{B} = \frac{mv_{\perp}^2}{2B} \quad . \quad (I-8)$$

Magnetic Mirrors

Quite a number of geometries for magnetic confinement exist.¹² Attention here is centered on the magnetic mirror machine, which gets its name from the properties of a charged-particle orbit in its magnetic field. Such a machine may be represented by a pair of Helmholtz coils.^{13,14} In this configuration, the region between the coils has a virtually constant field which gradually increases in strength near either coil as it is approached along a field line.

Suppose that a charged particle moving in the mirror field has its velocity vector inclined at an angle θ with respect to the field lines. Thus,

$$v_{\parallel} = v \cos \theta \quad (\text{I-9})$$

and

$$v_{\perp} = v \sin \theta \quad (\text{I-10})$$

The angle, θ , is known as the particle pitch angle. The pitch angle and the field at the midplane of the mirror trap (that plane parallel the planes of the coils and half way between them) are denoted by θ_0 and B_0 . For slowly varying fields, μ is nearly a constant.¹⁵ Hence, by Equation (I-8) and Equation (I-10):

$$\frac{v_{\perp}^2}{B} = \frac{v^2 \sin^2 \theta_0}{B_0} \quad (\text{I-11})$$

Since energy is conserved:

$$\frac{mv^2}{2} = \frac{mv_{\parallel}^2}{2} + \frac{mv_{\perp}^2}{2} \quad (\text{I-12})$$

we may write

$$v_{\parallel}^2 = v^2 \left(1 - \frac{B}{B_0} \sin^2 \theta_0 \right) . \quad (\text{I-13})$$

As B increases near the mirror throat, the right side of Equation (I-13) goes to zero and the particle is reflected providing θ_0 is not too small. If θ_0 is too small, B never attains the value required to reflect the particle, and it drifts out of the mirror along a field line. B is a maximum in the throat of the coil, having a value there of B_t . The minimum pitch angle for reflection, then, is:

$$\theta_{\min} = \sin^{-1} \left(B_0/B_t \right)^{\frac{1}{2}} . \quad (\text{I-14})$$

All particles with $\theta < \theta_{\min}$ are in the so-called loss cone and are not contained by the mirror.¹⁶ For a mirror ratio (B_t/B_0) of two, $\theta_{\min} = 45^\circ$.

Mirror Confinement

The loss of particles from the loss cone of mirrors points to a serious problem for mirror confinement. Not only do particles with $\theta < \theta_{\min}$ escape, but more plasma is constantly being scattered into the loss cone by Coulomb collisions between charged particles. The time required for a particle of charge ± 1 to be scattered 90° by long-range interactions with similar particles is¹⁷:

$$t_{\text{sc}} = \frac{(2m)^{\frac{1}{2}} (3T/2)^{\frac{3}{2}}}{4\pi e^4 n \ln \Lambda} . \quad (\text{I-15})$$

In this equation T refers to the kinetic temperature of the particles in ergs, and Λ is given by:

$$\Lambda = 3 hT/e^2 . \quad (\text{I-16})$$

These formulas apply to either ions or electrons. Therefore, a hydrogen plasma with $n_i = n_e \sim 3 \times 10^{11} \text{ cm}^{-3}$, $T_i \sim 0.1 \text{ eV}$, and $T_e \sim 10 \text{ eV}$ would have $t_{sc} \sim 1.6 \times 10^{-7} \text{ sec}$ for hydrogen ions and $t_{sc} \sim 1.8 \times 10^{-6} \text{ sec}$ for electrons. Obviously, the loss cone is being filled continually by Coulomb scattering in the remaining part of the plasma.

Yet there is another, more serious problem for confinement in mirror traps--plasma instabilities. These may be classified into three groups in mirror machines: hydromagnetic, kinetic, and drift instabilities.¹⁸ The first of these includes the hydromagnetic interchange (flute) instability. It is instigated by the manner in which ions and electrons drift apart in the radially decreasing field of the mirror trap. The plasma can be ejected to the walls of a mirror machine in the form of flutes or ridges in the plasma which extend along the field lines and grow in time.¹⁹ The other categories of instabilities are coupled to the deficiency of particles, trapped in a mirror machine, which have small values of perpendicular energy. These populations have more perpendicular energy than an equal population which is in thermal equilibrium. If the excess perpendicular energy can be transferred to electric field waves (with angular frequency $\omega > \omega_c$ for ions) propagating in the plasma, the wave amplitude may grow large enough to destroy confinement for much of the plasma.²⁰

Nevertheless, mechanisms exist to stabilize mirrors under special circumstances.^{21,22,23} The flute modes in particular appear to be mitigated by an increase in neutral pressure--and therefore an increase in cold-plasma density. Given metal end walls to the mirror trap, the cold plasma provides for higher conductivity to the end walls, which stops charge separation, and hence, the build-up of flutes. This effect is

known as "line-tying".²⁴ Increased plasma pressure is also suggested theoretically to alleviate instabilities due to temperature anisotropy, i.e., when the perpendicular energy is greater than the parallel energy.²⁵

ELMO

The ELMO experiment at the Thermonuclear Division of Oak Ridge National Laboratory is basically a magnetic mirror.²⁶ It operates in a time-independent manner, stabilized by line-tying to conducting end walls.²⁷ Figure 1 shows a cut-away view of ELMO. Electrons are heated by microwaves at resonance with their cyclotron frequencies.²⁸ Having been heated, they are capable of further ionization of both neutral particles and ions. Indeed, a variety of multiply charged ions (up to six times ionized or more) has been detected^{29, 30} using argon as a feed gas. The heated electrons are also capable of the excitation of all atomic species present which have one or more bound electrons. Given this excitation, each atom or ion radiates its own set of spectrum lines.³¹ Consequently, this radiation, which is a steady-state phenomenon in ELMO, makes possible a spectral analysis.

C. SPECTROSCOPY AS A PLASMA DIAGNOSTIC

Plasma diagnostics span a surprisingly broad range of physics. The most common techniques include the use of electric and magnetic probes, microwaves, lasers, photography, pressure and heat-sensitive probes, and spectroscopy. The latter is a wide field by itself, encompassing radiation from X-rays to the infrared.

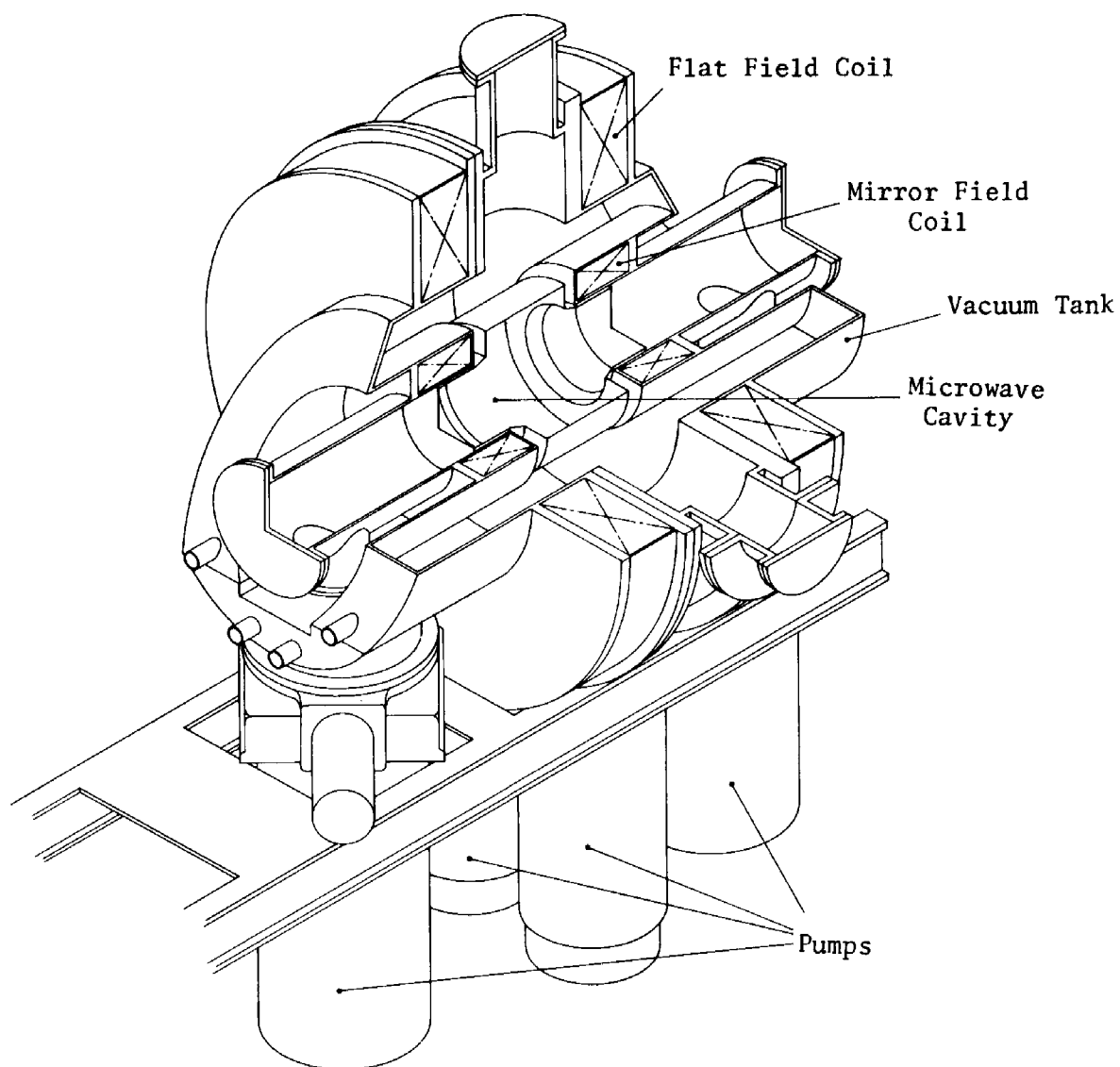


Figure 1. A Cut-away View of ELMO.

Plasma Spectroscopy

The spectral analysis is useful as a diagnostic in answering the basic questions concerning any plasma. One would like to determine which atomic species are present--whether different states of ionization or simply impurities. The usual thermodynamic variables, densities of plasma components, ion and electron temperatures, are sought. There are two inherent advantages in using spectroscopy in a plasma study. The first is that the spectrometer does not intrude within the boundaries of the plasma; therefore, the plasma is not perturbed by its presence. The second is that, given a reasonable theoretical model, a plasma spectrum holds answers to a great number of the above inquiries about plasma parameters.³²

This is not intended to imply that there are no disadvantages. Perhaps the greatest drawback is the validity of the theoretical model as is seen in the next subsection. A second problem is that a spectroscopic signal is integrated along the optical path through the plasma. If the plasma is inhomogeneous, only special geometries allow local intensities to be calculated.³³ Other difficulties will become manifest in the course of this dissertation.

The wavelength region of interest for this dissertation, a spectroscopic investigation of a neon plasma in ELMO, is 200 Å to 1300 Å, the so-called extreme ultraviolet (XUV). The reason for such a choice is that the line radiation of highly charged ions occurs in the XUV.³⁴ As mentioned before, such ions are abundant in the plasma in question; so there is much to be seen.

Plasma Model

The theoretical model devised to interpret spectral information is critical. Out of the multitudes of possible atomic processes, those dominant must be incorporated into the model. The reliability of plasma parameters then derived from the model depends on the consistency of the model with the actual physical state of the plasma.³⁵

The ambition of this thesis is to construct a model for the excitation and ionization of the ELMO neon plasma from what knowledge is recorded in the scientific literature and from observations made during the present experiment. This being done, the spectroscopic measurements may be converted into plasma variables of interest. In this case, these are the electron temperature, the densities of neutral neon and of different ions of neon in the plasma, the electron density, and the ion temperature. Finally, the model can be refined and relevant questions answered--for example, an understanding of the dominant modes of ionization may be gained.

D. AN OUTLINE OF THE DISSERTATION

The body of this dissertation is divided as follows:

Section II is a review of the ELMO plasma. Settings of experimental variables, e.g., pressure, magnetic field, and microwave power, are listed along with past measurements from the scientific literature of density, temperature, and ionic composition.

The important third section enables the interpretation of the experimental measurements. A theoretical physical model is discussed. The necessary assumptions concerning the electron plasma, ion containment,

excitation and ionization modes are listed. Given the model, the theory is expounded which allows derivation of the plasma parameters by a spectroscopic study.

Section IV consists of the experimental considerations taken in order to collect the spectroscopic data. First is a description of the spectrometer used: its grating, mounting and alignment, vacuum system, etc. Next is a description of the photon detector and its accompanying circuitry. This is followed by a subsection on the spectrometer calibration--both its wavelength calibration and its intensity calibration. Finally in Section IV, the output of data is described. The spectrometer dispersion and resolution are compared. Factors influencing signal amplitude are discussed.

Section V includes the results of all spectroscopic observations and translation of these measurements into hard plasma parameters by the methods of Section III. Following a tabulation of the measured line radiation comes a subsection dealing with electron temperature measurement. After this, the population densities of the various states of ionization and the electron density are deduced. The ion temperature estimate is introduced next, and finally, error analysis is considered.

The last section, Section VI, details the relationship between the present assessments and those of previous workers. The physical model of this thesis is examined to see how well it stands. Remarks on possible applications of techniques herein demonstrated are made, and, in closing, suggestions for future work related to this dissertation are rendered.

II. A REVIEW OF ELMO PLASMA PARAMETERS

This section includes a review of plasma parameters in the ELMO device. These parameters are divided into two types: those directly controlled by the researcher, which shall be called experimental variables, and those over which there is no direct control, the value of which may be altered only by manipulating the experimental variables. Parameters of the second type are ingrained in the plasma, and they shall be called intrinsic variables.

A. EXPERIMENTAL VARIABLES

In most experiments, certain co-ordinates are subject to the scientist's discrimination. These he may change by the twist of a knob or the flip of a switch. In the formation of a mirror-contained plasma in ELMO, the researcher must decide what gas and gas pressure to use, what magnetic field, and how much microwave power.

Pressure

The gas which forms the plasma in ELMO is regulated by a servo-mechanism which maintains the pressure in the 16 liter microwave cavity at a value selected by the experimenter. Feedback from a Bayard-Alpert type vacuum ionization gauge³⁶ controls the opening and closing of a valve on the gas-feed line. Vacuum is held by four oil diffusion pumps--two 6 inch pumps directly under the machine (Figure 1) and a 10 inch pump under each end. A freon cold trap refrigerates the diffusion pumps

to reduce the back-streaming of pump oil, water and other vapors. Mechanical roughing pumps remove the exhaust of the four diffusion pumps.

The feed gas, supplied in standard gas cylinders may be any of several varieties--generally hydrogen, helium, argon, or deuterium. Of course, there is the option of operating with air. For the present experiment, research grade neon (minimum purity > 99.998%) was used.

The key element of the pressure control system is the ionization gauge. Since different gases induce different behavior from the gauge on account of their various ionization potentials, a gauge correction is necessary. Let S_1 be the gauge sensitivity to gas #1, and S_2 similarly for gas #2. A given current in the tube gives a constant meter deflection regardless of the gas present. If readings are taken separately on two gases at pressures P_1 and P_2 which produce the same gauge deflection, and if the gauge current is below the saturation level (in the region where the gauge deflection is linearly related to pressure), then

$$P_1 S_1 = P_2 S_2 \quad . \quad (II-1)$$

The S values have been measured by Dushman and Young who claim that there is little difference between different kinds of gauges.³⁷

The ionization gauge which regulated ELMO is supposedly calibrated on air, i.e., on N_2 . A gauge pressure equivalent of 6×10^{-6} Torr of air (N_2) was selected for this experiment. By Equation (II-1), this transforms into 2.5×10^{-5} Torr for neon, which was compatible for stable operation of the mirrors. The pressure was not varied during the course of the experiment.

Magnetic Field

As can be seen in Figure 1, the microwave cavity where the plasma is formed is between two mirror coils. Outboard of these are two other coils--referred to as flat-field coils--which reinforce the mirror field. The total current, 3800 amperes for this experiment, is supplied to the water-cooled coils by a 2 megawatt motor generator. This gives a typical mirror field profile (Figure 2), which has a field on the order of 8 kG on axis in the midplane and of about 16 kG on axis in the mirror throats. Hence, the mirror ratio is equal to two and the critical pitch angle [Equation (I-14)] is 45° .

Microwave Power

From Equation (I-7) we see that the cyclotron frequency of an electron in ELMO varies between $1.4 \times 10^{11} \text{ sec}^{-1}$ and $2.8 \times 10^{11} \text{ sec}^{-1}$. If an electron comes into resonance with an electric field, it can be accelerated or heated by that field. This effect, electron-cyclotron heating or ECH, has been reported in a number of experiments besides ELMO.^{38, 39} The microwave frequency of 35.7 gigahertz, having an angular frequency of $2.24 \times 10^{11} \text{ sec}^{-1}$ and a wavelength of 8.4 mm, is seen to correspond to ω_c when $B = 12.8 \text{ kG}$. On a particular surface in the microwave cavity (Figure 3) for which the magnitude of the field is constant and equal to this value, electrons undergo ECH.

Microwave power is supplied by a travelling wave tube oscillator with a variable output of up to one kilowatt. All data in this experiment were taken with a microwave power level of $800 \pm 50 \text{ watts}$.

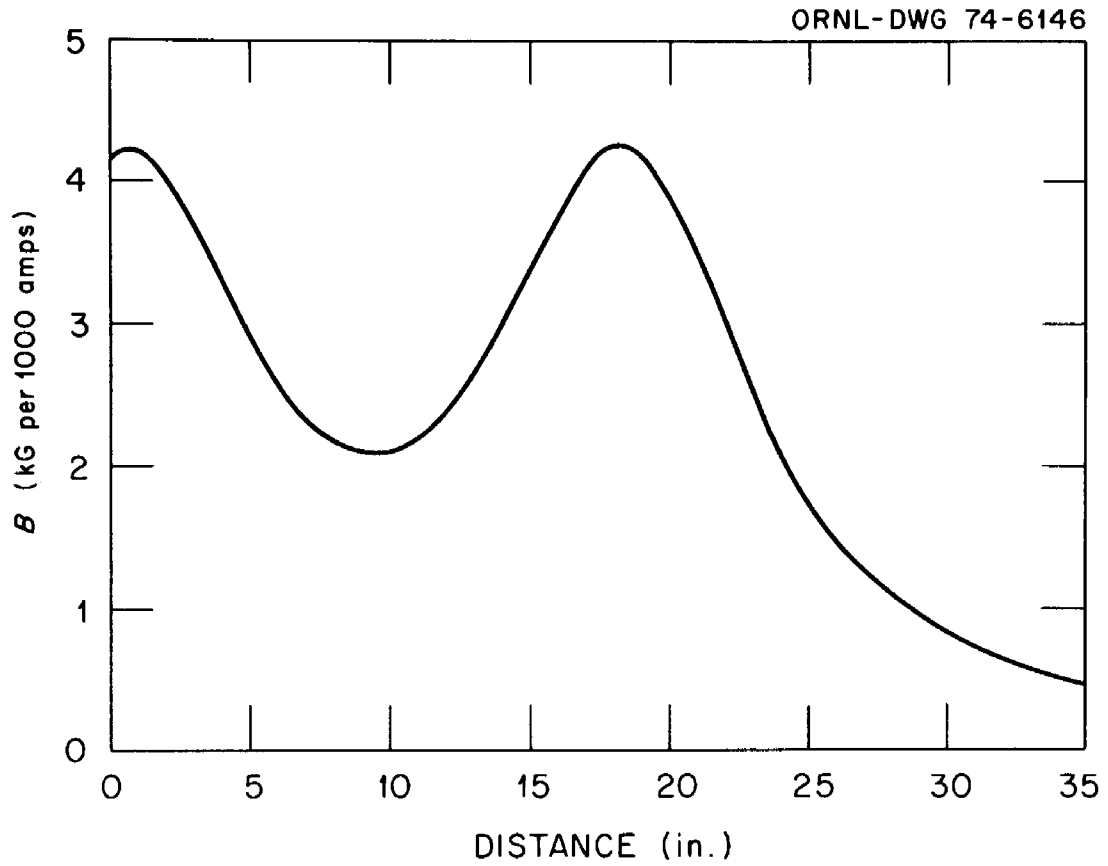


Figure 2. ELMO Magnetic Field On Axis per 1000 Amperes Total Current versus Distance from One End of the Microwave Cavity.

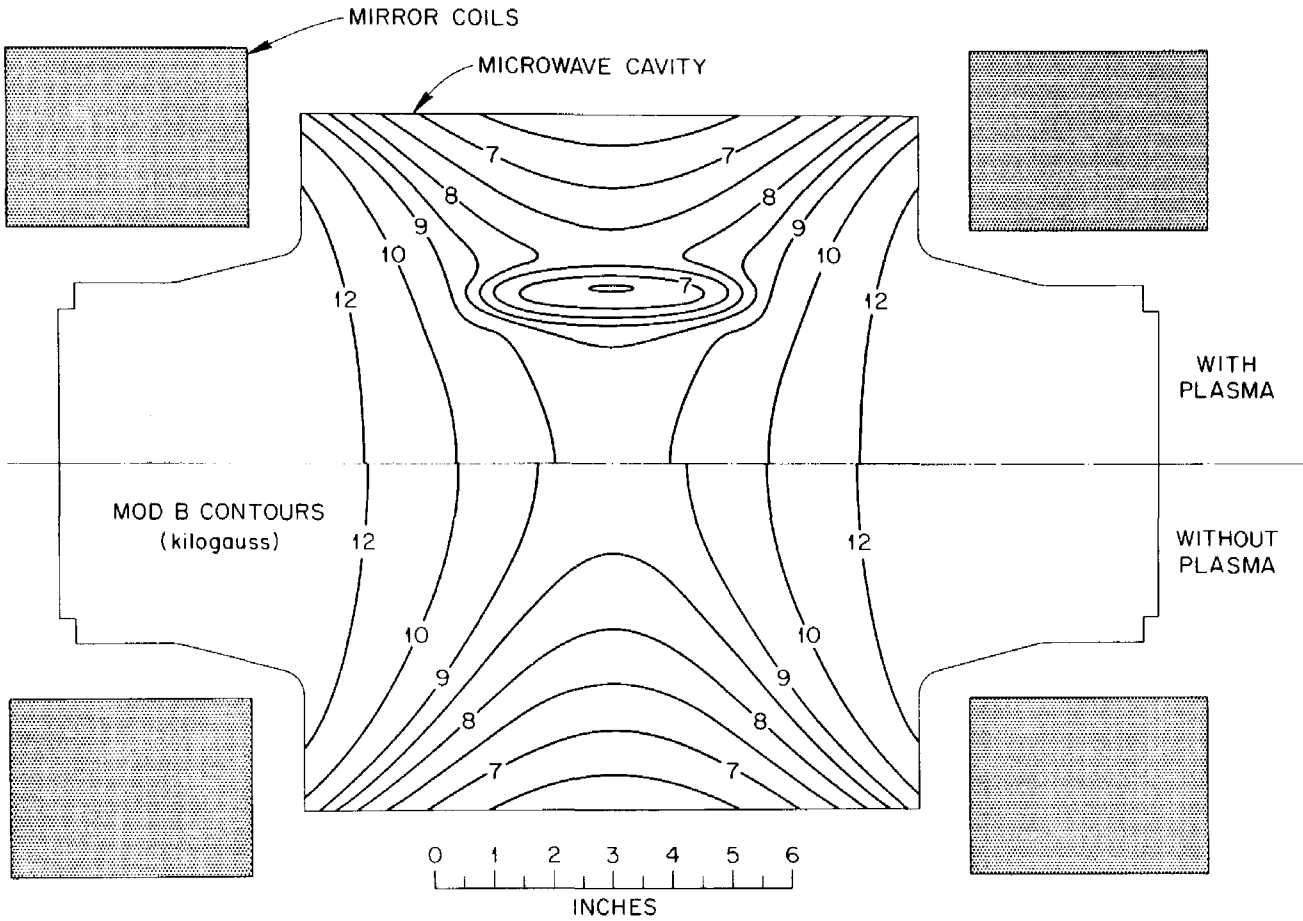


Figure 3. Mod-B Contours for ELMO System with Plasma Profile Derived from Diamagnetic Data.

B. INTRINSIC VARIABLES

We come now to the intrinsic plasma variables. They are unknowns which must be discovered by whatever diagnostics are available; to measure these parameters is the objective of plasma physics. These functions of the experimental variables include densities of plasma components, their temperatures, particle containment times, fractional ionization, etc. Below is a summary of results from ELMO plasmas under an assortment of conditions.

The Electron Plasma

One of the most interesting things about the entire ELMO project is the high temperature attained by electrons via ECH. In experiments using D₂, Dandl⁴⁰ and Edmonds⁴¹ reported a hot-electron plasma of mean energy 750 keV and density several times 10¹¹ cm⁻³. This plasma assumed the shape of an annulus around the machine axis which filled the central portion of the cavity. The closed lines of constant magnetic field intensity (mod-B contours in Figure 3) indicate the approximate position of the hot-electron ring. The radius of the plasma ring is approximately 9 cm, and the thickness of the shell is between 3 and 4 cm. With a net length of 10 cm, this plasma has a volume on the order of two liters. The containment time of the hot electrons after microwave turnoff is on the order of 200 msec. The experimental variables of these measurements were: a filling pressure of practically 10⁻⁵ Torr (gauge), a field of 8 kG on axis in the midplane with a mirror ratio of 2.2, and 2 kW of 8-mm microwave power.

Simple ECH is not the only heating mechanism at work in the plasma. Work by Dandl⁴² has shown that a higher frequency microwave component superimposed on the primary resonance frequency produces a very energetic electron plasma ring. Mean energies of 1.5 MeV and densities of 10^{12} cm^{-3} were achieved by this effect, known as upper-off-resonance heating or UORH. Energy stored in the plasma ring was measured at 360 joules--a factor of about 15 above the case with no off-resonance power. Even without the second microwave frequency, there is some degree of UORH because of Doppler shifts of the resonance microwave frequency and the relativistic mass increase of the hot electrons.⁴³

The stability of the plasma, as stated in Section I, depends on a cold background plasma for line-tying. Besides the annular plasma, earlier work on ELMO⁴⁴ points to the existence of at least two other energy groups of electrons under similar experimental conditions: D_2 at 1.25×10^{-5} Torr, a mirror ratio of 2.2 with a central field of 8.5 kG, and 2 kW of 8-mm microwave power. Intrinsic parameter values for the warmer of these groups are: temperatures of 15 to 30 keV, densities of up to $5 \times 10^{11} \text{ cm}^{-3}$ depending on the mirror ratio, and a distribution more or less uniform throughout the cavity. The colder electron plasma is more dense--approximately 10^{12} cm^{-3} --and is spread evenly in the available volume. Its decay time at microwave turnoff is 80 to 100 μsec . No direct temperature measurements were made, but that quantity was estimated to be a few tens of eV.

Three items need to be taken into account in order to modify correctly the electron plasma so far described so that it matches that of the present experiment. Each of these involves an experimental variable.

First is the obvious change in the feed gas: neon instead of deuterium. Values of electron temperatures and densities quoted so far all apply to a deuterium plasma. Previous experience with xenon⁴⁵ indicates that a high-Z gas reduces both the mean energy and the number of hot electrons in the plasma. Presumably, neon with an atomic weight ten times that of deuterium will induce a similar effect on the electrons.

Secondly, as mentioned, only 800 watts of microwave power are used compared to 2 kW in cited experiments. Dandl's measurements for both ECH⁴⁶ and UORH⁴⁷ show a reduction of stored energy and, thus, of the density of energetic electrons with the lowering of microwave power.

Third and finally, the mirror ratio is currently 2.0 as opposed to 2.2 as in the quoted material. This may account for an additional 30% falloff in the hot-electron density.⁴⁸

The Ion Plasma

Detailed information concerning ions in ELMO is lacking. However, by the condition of electrical neutrality,

$$N_e = \sum_{k=1}^Z k N_k \quad , \quad (\text{II-2})$$

where N_e is the total number of electrons in the plasma, N_k the number of ions of charge k , and Z the atomic number of the feed gas. (To be completely correct, impurities in the plasma should be included by summing over different Z 's.) One of the aims of this thesis is to measure densities of the various charge states in a neon plasma where $Z = 10$.

The ions are very cold because of the low rate of energy transfer from electrons.⁴⁹ Consequently, their temperature is given roughly just by their thermal energy.⁵⁰ Because of this, their confinement time in

the plasma is short compared to the electrons--perhaps a single time of flight along a field line.⁵¹ (A neon ion at room temperature would take about half a millisecond to travel across the cavity at constant velocity.) The reason for the short confinement is suggested by Equation (I-15). Thermal neon ions by this formula undergo 90° scattering in approximately 0.1 μsec in the absence of a magnetic field. Even with a strong field, the loss cone is apparently being filled by ions at a rapid, steady rate.

As an example, the time to raise the ion temperature 1 eV by electron collisions is calculated. Suppose $T_e \sim 10$ eV and $n_e \sim 3 \times 10^{11}$ cm⁻³. (Implicit in this exercise is the assumption that $T_i < T_e$.) Assuming a Maxwellian distribution of electrons, the heating rate is given by⁵²:

$$\frac{\Delta T_i}{\Delta t} = \frac{4\pi n_e e^4}{(27 m_e T_e)^{\frac{1}{2}}} \frac{m_e}{m_i} \ln \Lambda \quad . \quad (\text{II-3})$$

For the above conditions, singly ionized neon is heated 75 eV/sec. Therefore, such particles must be contained 13 msec to be heated even 1 eV above room temperature. The heating due to warmer electron distributions is even slower because of the $T_e^{-\frac{1}{2}}$ dependence. Clearly ions will be cold unless confinement is improved.

The degree of ionization in a high-Z gas in ELMO is such that it has been proposed as an ion source for producing transuranic elements by the fusion of heavy nuclei.⁵³ Van der Woude⁵⁴ has used a time-of-flight spectrometer to examine the charge-to-mass ratio of ions drifting through a hole in the end plate. Using argon as a feed gas, he has detected Ar⁴⁺

with a high degree of certainty and probably Ar^{5+} and Ar^{6+} also. Later, with a much improved mass spectrometer Dandl⁵⁵ found evidence of neon-like argon, i.e., Ar^{10+} . Although Ar^{9+} and Ar^{10+} have charge-to-mass ratios similar to high charge states of some common impurities in the plasma (N^{3+} , O^{4+} , C^{3+}), the identity of Ar^{8+} is much more definite.

III. THE PLASMA MODEL: THE LINK BETWEEN THEORY AND EXPERIMENT

This section introduces the physical models for excitation and ionization in a neon plasma. Afterwards, these models are used to evaluate intrinsic plasma variables in terms of the intensities of the line radiation emitted by the different atomic and ionic species present in the plasma.

A. THE EXCITATION MODEL

First is the introduction of the usual kinds of plasma models. From these the excitation theory for the present experiment is taken. Within that selection there are many ways to populate excited states of atomic systems. The dominant process of these several modes is singled out, and expressions given which relate the various intrinsic parameters to experimental observables.

Common Plasma Models

The least difficult plasma models embrace the assumption that the plasma is "optically thin," i.e., that the plasma radiation does not interact with the plasma and escapes with no attenuation. Offered here is a simple calculation on which to base this assumption for the ELMO plasma. The mean free path of a photon before absorption is given by the inverse of the absorption coefficient:

$$l_{MF} = \alpha^{-1} = \frac{1}{n\sigma} \quad , \quad (III-1)$$

where σ is the cross section for photon absorption. The value of σ may be estimated as πa^2 , where a is the radius of a neon atom, about 1 \AA .⁵⁶ In ELMO, with $n \sim 10^{12} \text{ cm}^{-3}$, $l_{MF} \sim 3200 \text{ cm}$ --much longer than the optical path in the plasma. Thus, the ELMO plasma is considered optically thin. Another check on this assumption is discussed in Section V, where the phenomenon of resonance self-absorption is considered. This effect makes itself manifest by the absorbing of a photon representing an atomic transition to the ground state by a similar atomic system which is then raised to the same excited state as the original system.

Now, depending on the thermodynamic properties of the plasma, one of several models may be chosen. These are: (1) the local thermodynamic equilibrium model (LTE), (2) the corona model, and (3) the collisional-radiative model (CR).

Of the three models listed, the LTE plasma comes closest to complete thermodynamic equilibrium in which every process is balanced by its inverse. Because radiative decay has no inverse in an optically thin plasma, LTE can be applied only if particle collisions dominate the distribution of populations of atomic energy levels.^{57, 58} The density of electrons required for this is several orders of magnitude above that reported in Section II for ELMO.

The corona model is not restricted by the detailed balancing of every process in the plasma, e.g., the emission and absorption of radiation. Furthermore, this approach holds for plasmas of much lower density than those to which LTE applies so that only the strongest collision events are considered. In this case, only the ground states of atomic systems will be significantly populated.⁵⁹

The CR model is a blend of the other two models which implies intermediate densities. Populations of states are determined by both radiative and collision processes. However, for mathematical tractability, a certain quantum level is picked, above which the radiative effects are disregarded and the statistical nature of LTE retained.⁶⁰

For the ELMO plasma, the LTE model is already discarded. To decide between the corona model and the CR model, one must inquire as to the time available for an excited atom or ion to undergo an inelastic collision with an electron or other particle. This time is just the natural lifetime of the excited state, τ^* . For the j th state:

$$\tau_j^* = \frac{1}{\sum_{i < j} A_{ij}}, \quad (\text{III-2})$$

where A_{ij} is the probability per unit time of a spontaneous transition to the i th level--the transition probability. If τ^* is small compared to the mean-free-time between inelastic collisions, t_{MF} , then the excited state should decay by emitting a photon before any collision takes place. Usual time scales for τ^* are 10^{-8} or 10^{-9} sec.⁶¹ The value of t_{MF} is given by:

$$t_{MF} = \frac{1}{n\sigma v}, \quad (\text{III-3})$$

where σ is now the inelastic collision cross section. We may take the same value for $1/n\sigma$ as was found in (III-3), i.e., 3000 cm. In ELMO, $v \sim 10^{10}$ cm/sec for fast electrons; therefore, t_{MF} is easily as large as 3×10^{-7} sec. Only long-lived metastable levels will concern us (and then only if their density is of the same order of magnitude as the ground state density). With this proviso then, τ^* is less than t_{MF} ,

and the corona model is seen to be a suitable approximation for the ELMO plasma.

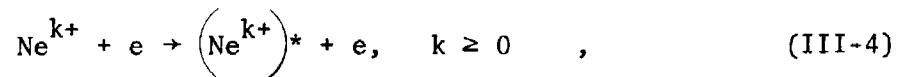
Methods for Populating Excited States

Several routes for the populating of excited states in atoms or ions ensue collision events. These include atom-atom and atom-electron interactions. In any case, the excitation is an inelastic process which requires the responsible mechanism to convert a specified amount of kinetic energy to potential energy: the so-called excitation energy, E_x . E_x represents a threshold for excitation; if the available kinetic energy is less than E_x , no excitation can occur.

A second course contributing to excited populations is cascade feeding. A level is filled in this way by a transition from a higher energy level. Additional possibilities are ionization events in which the new ion is left in an excited state, and ionic recombination in which the new system is excited thereafter.

Model Simplification

The more of the possible excitation modes which can be neglected the simpler the model becomes. Fortunately, most of the above are negligible. In fact, of all the excitation schemes, the only one considered to be of significance is electron-impact excitation:



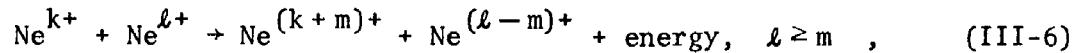
where the ionic charge is k and the asterisk implies an excited state.

If the cross section for electron-impact excitation is σ_x , then the excitation rate for this process is

$$S_x = \int_0^{\infty} v \sigma_x(v) f(v) 4\pi v^2 dv, \quad (\text{III-5})$$

where $f(v)$ is the electron velocity distribution function. S_x will be analyzed in the next subsection.

Atom-atom collisions are neglected completely. The mean kinetic energy of atomic systems in ELMO is much less than E_x . The impact of two neutrals for instance cannot cause excitation. The exothermic charge-exchange collisions,



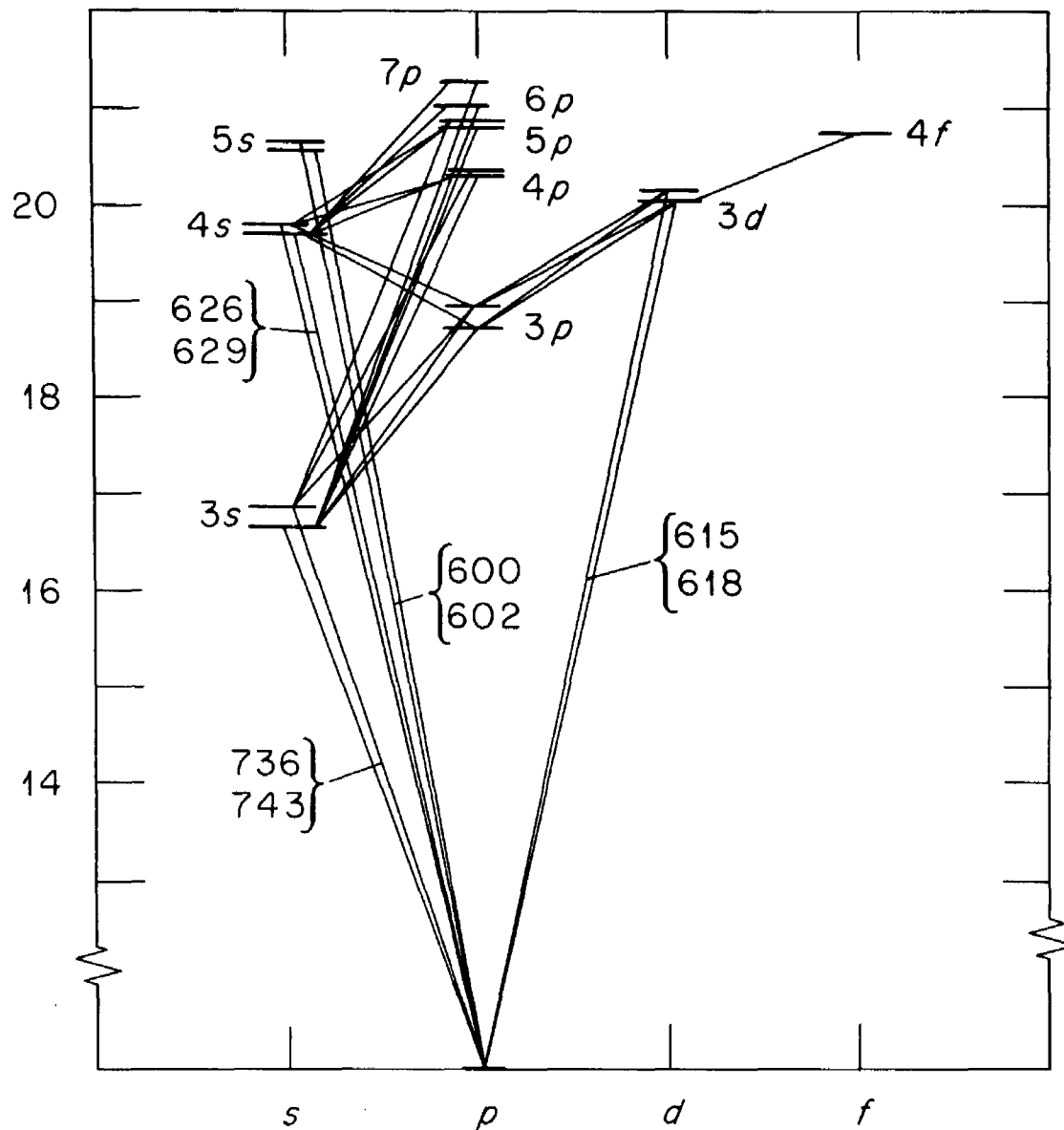
could leave one of the reaction products in an excited state, but for the following reasons, these processes are ignored. Recall that the ions in ELMO are very cold. Unless k is zero, that is, unless one of the reactants is a neutral particle, the relative kinetic energy is insufficient to cross the Coulomb barrier between the two systems and charge exchange is impossible. For another case, assume that $k = 0$ and $l = m$, the condition of symmetrical resonance charge exchange. Now there is no energy for excitation on the right side of Equation (III-6). The possibility that one of the reactants is initially excited and could transfer that energy to a reaction product is small because of the short lifetimes of most levels. Even if an incoming particle is in a metastable state, these levels are not usually energetic enough to supply E_x for an allowed transition (see Figures 4 through 8). What is left is the case for $k = 0$ and $l > m$. Little is known about charge-exchange cross sections, $l, 0 \sigma_{m, l-m}$, in gases at thermal energies. However, for the case $l = 2$ and $m = 1$, Hasted and Hussain⁶² presents $20 \sigma_{11}$ as a nearly flat function near 10^{-17} cm^2 for the energy range from 400 to 3600 eV. The charge-exchange rate is calculated by

$$S_{\text{CX}} = \int_0^{\infty} v \, l, 0 \sigma_{m, l-m}(v) F(v) 4\pi v^2 dv, \quad (\text{III-7})$$

where $F(v)$ is an ion velocity distribution function. If ${}_{20}\sigma_{11}$ does not increase at lower energies, the charge-exchange rate will be small compared to the electron-impact excitation rate, S_x . (Note that mere charge exchange does not guarantee excitation.) In conclusion, all atom-atom encounters are neglected in this model.

Cascade feeding is possible whenever the higher energy levels of an atomic system are populated. Figure 4 shows a simplified term diagram for Ne I, neutral neon, which indicates the cascade filling of the upper levels of the most intense UV transitions. The key to minimizing this problem is a judicious choice of the transitions to be used in the model. In the UV spectrum of Ne I, the amount of feeding should increase with wavelength. The upper levels of the shorter wavelength transitions are nearer the continuum so that there are fewer states which may feed them. For Ne I, then, the idea is to choose the shortest wavelength line possible. With other neon systems, some levels are apparently not fed at all, e.g., the lowest ${}^3P^0$ level in Ne III, doubly ionized neon (Figure 6). Still other levels are fed by other UV transitions which may be measured with the same spectrometer (Section IV) as the line of interest. As is seen in Section V concerning line intensities, cascading plays a minor role where it is evident; thus, the assumption is made that the same is true where the degree of cascade feeding has not been measured.

IONIZATION POTENTIAL 21.56 eV



ORBITAL ANGULAR MOMENTUM QUANTUM LEVELS
OF THE EXCITED ELECTRON

Figure 4. A Simplified Term Diagram of Ne I Showing the Cascade Feeding of the Strongest UV Transitions.

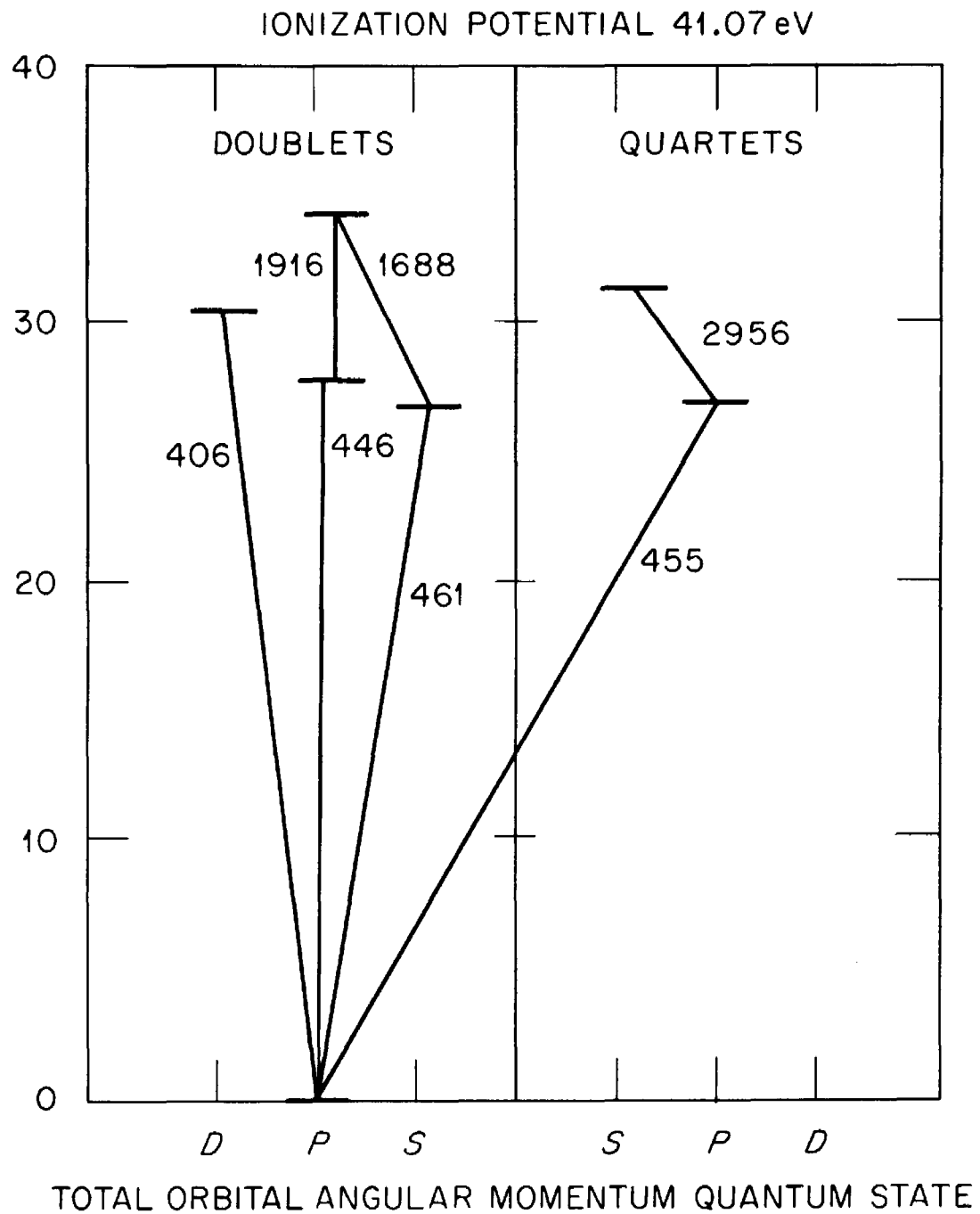


Figure 5. A Simplified Term Diagram of Some UV Transitions in Ne II--Wavelengths in Angstroms.

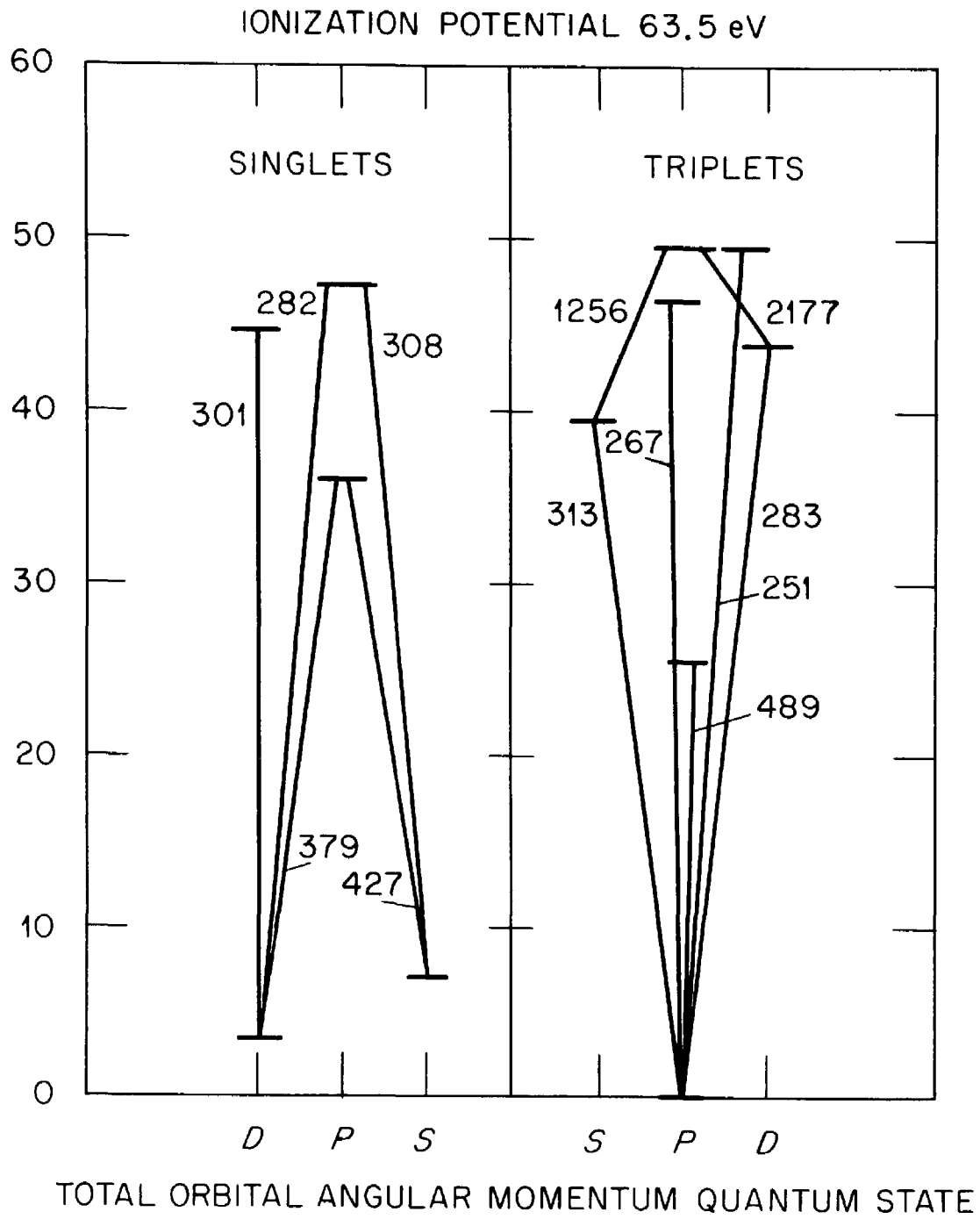


Figure 6. A Simplified Term Diagram of Some UV Transitions in Ne III--Wavelengths in Angstroms.

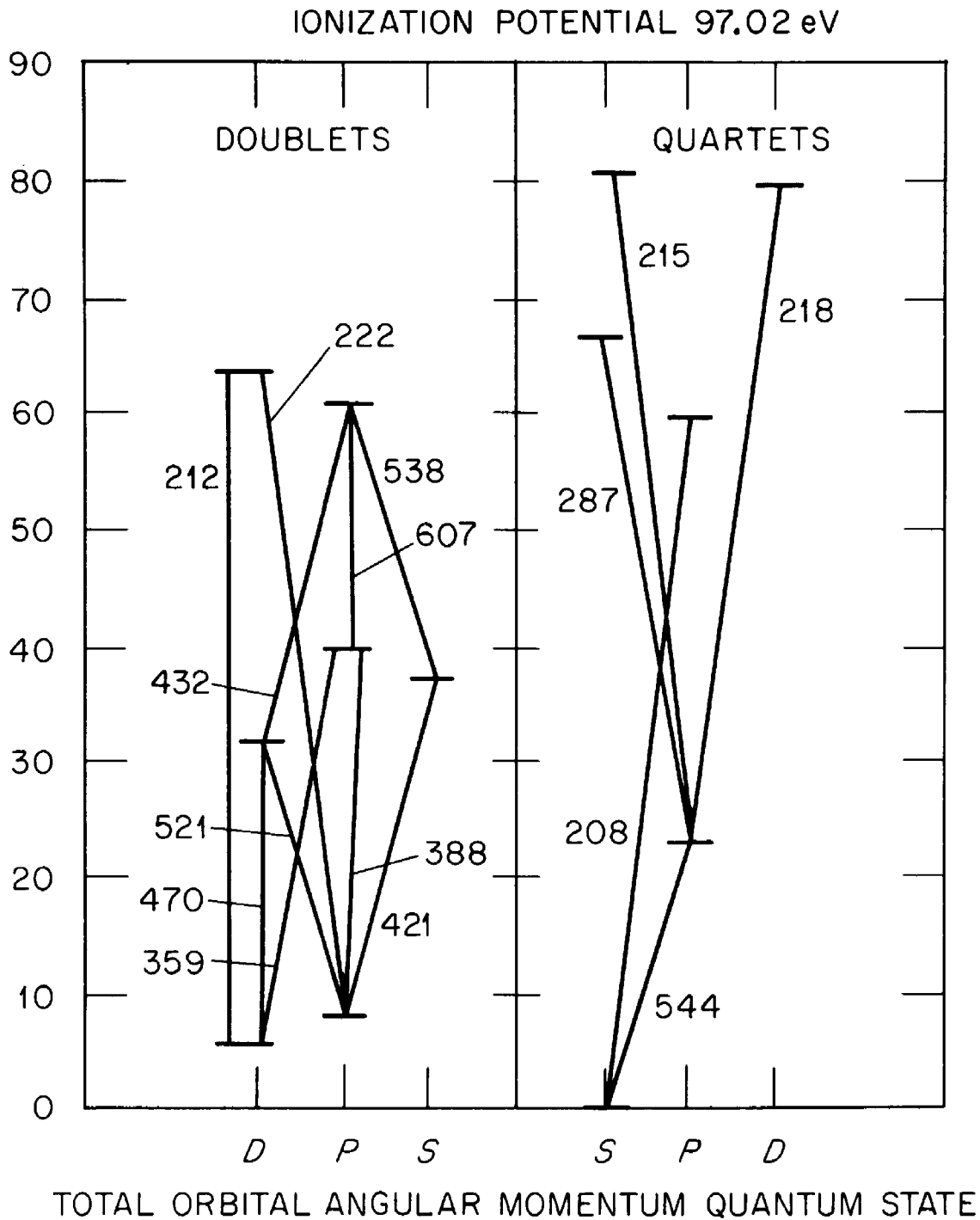


Figure 7. A Simplified Term Diagram of Some UV Transitions in Ne IV--Wavelengths in Angstroms.

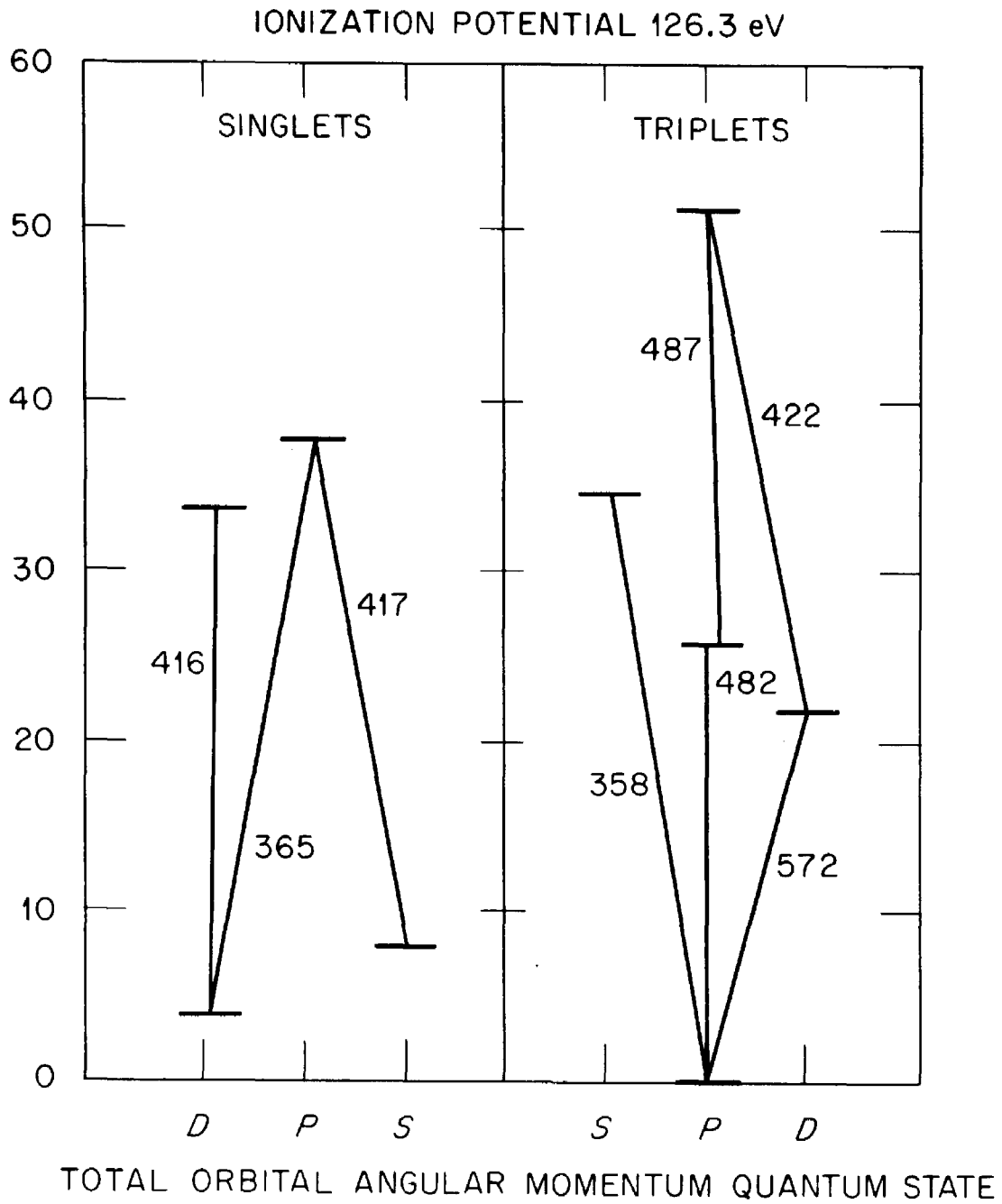
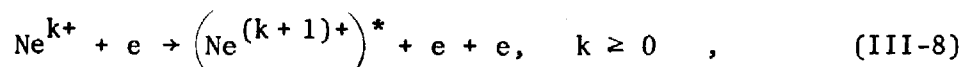


Figure 8. A Simplified Term Diagram of Some UV Transitions in Ne V--Wavelengths in Angstroms.

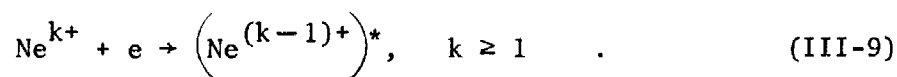
Simultaneous ionization and excitation,



is yet another means for the occupation of excited states. Again, little data are available for this process. Lamb and Skinner⁶³ have studied the production of excited He^{1+} from neutral helium bombarded by electrons of several hundred electron volts. They report that in about nine percent of the ionizing collisions, the ion is left in an excited state. Of these about one part in nine is in a metastable level while the rest decay to the ground state. We shall assume a similar result for the ionization of ground-state neon systems.

Suppose now that the atomic system on the left side of Equation (III-8) is a metastable. Koozekanani has done theoretical work on neutral argon initially in a metastable state.⁶⁴ He finds that the cross section for simultaneous ionization and excitation of a metastable neutral is perhaps a tenth that for ionization alone, depending on which metastable level is considered. If the neon results are consistent with this study, we assume that neglect of all such events [Equation (III-8)], regardless of the initial state, is a fair simplification.

Finally is electron-ion recombination:



The recombination rate, α , which follows from Equation (III-5) if σ_x is replaced by the cross section for recombination, is given by McWhirter⁶⁵ as:

$$\alpha = 2.6 \times 10^{-13} k^2 / T_e^{\frac{1}{2}}, \quad (\text{III-10})$$

where the units of α are cm^3/sec and T_e is in eV. Though the reliability

of this expression is $\pm 100\%$, for $k < 5$ we shall see that recombination may be safely neglected. For reference purposes, suppose $T_e \sim 10$ eV. Then for four-times ionized neon, $\alpha \sim 1.3 \times 10^{-12}$ cm³/sec.

The Electron-Impact Model

We have seen a great deal of simplification so far, but the details of electron-impact excitation must still be handled. Two items especially demand attention. The first is the initial state of the atomic system to be excited. This will be dealt with next and then the second problem, the dependence of S_x on the electron velocity distribution [Equation (III-5)].

It has been previously stated that excitation is initiated in either the ground state or a long-lived metastable state. The contribution of metastables depends on their population relative to the ground state. Consistent with a corona model for low-density plasmas, the assumption is made that no metastable level is sufficiently populated to influence excitation. We shall consider, then, only excitation from the ground state.

Since in Section II we learned of the complex temperature groups of electrons in ELMO, further reduction of the problem is desirable. In view of the low density and small volume of the annular plasma, its contribution to $f(v)$ is ignored. The assumption is now made that S_x consists of two parts:

$$S_x(\epsilon) = S_x(C) + \epsilon S_x(H) \quad . \quad (III-11)$$

The letter "C" in parenthesis implies the cold background electron plasma; "H" implies the 15 to 30 keV component. Both plasmas are

assumed to be uniform throughout the cavity; ϵ is the ratio of electron densities, hot to cold:

$$\epsilon = \frac{n_H}{n_C} \quad . \quad (\text{III-12})$$

It is expected that ϵ will be a small number, certainly less than one.

The form chosen for σ_x depends on whether the atomic system to be discussed is an ion or a neutral. Hinnov⁶⁶ gives these as:

$$\sigma_x(\text{neutrals}) = \frac{\sigma_o e^{\ell n} U}{U} \quad (\text{III-13})$$

and

$$\sigma_x(\text{ions}) = \frac{\sigma_o e^{\ell n} 2U}{U} \quad . \quad (\text{III-14})$$

U is the electron energy E divided by E_x , and e is the base of the natural logarithms introduced as a normalization factor. The cross section, σ_o , is defined as:

$$\sigma_o = \pi a_B^2 f \left(\frac{E_H}{E_x} \right)^2 \quad , \quad (\text{III-15})$$

where a_B is the Bohr radius, E_H the Rydberg energy, 13.6 eV, and f the absorption oscillator strength.

The cold-electron component is assumed to be Maxwellian. Then it follows that the excitation rate due to cold electrons with $y = E_x/T_e$ is:

$$S_x(C) = \sigma_o e^{\sqrt{\frac{8 E_x}{\pi m}}} y^{\frac{1}{2}} \Phi(y) \quad (\text{III-16})$$

and

$$\Phi(y) = \int_y^{\infty} \frac{e^{-x}}{x} dx + e^{-y} (\ell n 2) (1 - \delta_{0,k}) \quad . \quad (\text{III-17})$$

The Kronecker delta, $\delta_{0,k}$, k being the charge of the system to be excited,

causes the second term on the right of Equation (III-17) to vanish for neutral neon. [Equation (III-16) is given by Hinnov for $k \neq 0$ in the previous reference.]

For the hot-electron component, T_e is not precisely determined, only bound by the limits 15 to 30 keV; nor is the shape of $f(v)$ known. The approximation is made that:

$$S_x(H) = \sigma_x v \quad , \quad (\text{III-18})$$

where both quantities on the right are evaluated at a particular value of T_e . From the low to the high temperature limit, $S_x(H)$ as described by Equation (III-18) decreases by about 23% regardless of the value of E_x or the charge of the atomic system. Therefore, an intermediate value is arbitrarily picked for T_e --namely 20 keV.

Population Balance Equations

To summarize the excitation model, a corona model, we have direct excitation of all charge species from the ground state by electron impact. Excitation from metastable levels is neglected. Simultaneous ionization and excitation is ignored as is electron-ion recombination. Cascade feeding is judged to be negligible. Atom-atom interactions are disregarded, and of course, atom-photon encounters. All de-excitation is by spontaneous radiative decay.

The steady-state populations of levels (because ELMO is a steady-state device optically) require:

$$n_j \sum_{i < j} A_{ij} = n_C n_0 S_{xj}(\epsilon) \quad , \quad (\text{III-19})$$

where n_j is the population density of the j th level, n_0 the density of

the ground state, and $S_{xj}(\epsilon)$ the excitation rate for the j th level from the ground state.

The n_j values are related to experimental measurements as follows. Let I_{hj} be the number of photons per second of wavelength λ_{hj} from the j th level seen by the spectrometer. This quantity depends on the number of atoms in state j , the probability that a photon will be emitted, and the chance that it is directed toward the spectrometer. Hence,

$$I_{hj} = n_j A_{hj} \frac{TV\Omega}{4\pi} \quad , \quad (\text{III-20})$$

in which V is the volume of plasma visible to the spectrometer, Ω the corresponding solid angle, and T the transmission efficiency. Substituting in Equation (III-19) for n_j , one finds:

$$n_o S_{xj}(\epsilon) = \frac{4\pi I_{hj} \sum_{i<j} A_{ij}}{TV\Omega n_C A_{hj}} \quad . \quad (\text{III-21})$$

This important equation is the means by which the intrinsic variables are derived from experimental observations.

B. A DERIVATION OF INTRINSIC PARAMETERS FROM THE EXCITATION MODEL

Outlined now is the manner in which useful parameters--the cold-electron temperature, densities of charge states, and electron density--come out of this corona model.

The Cold-Electron Temperature

Consider Equation (III-21) in the event that two UV transitions are observed which belong to the same ion. Both originate from the same

ground state; the spectrometer sees the same volume and solid angle for both; the electron density which excites each level is the same. A calibration of the optics gives the relative weight of T as a function of wavelength. The intensities, I, are measured, and the A's for many transitions can be found in the literature (Section V).

After removing common factors and correcting for transmission and cascading, the ratio of excitation rates can thus be determined experimentally:

$$R = \frac{S_{xj}(\epsilon)}{S_{xl}(\epsilon)} = \frac{I_{hj} A_{kl} \sum_{i<j} A_{ij}}{I_{kl} h_j \sum_{i<l} A_{il}} \quad . \quad (\text{III-22})$$

Equations (III-16) and (III-18) are then used in (III-11) to calculate the temperature dependence of R for a family of ϵ 's. In principle, if ϵ is known, then where the experimental and theoretical values agree, the cold-electron temperature is determined.⁶⁷

The Densities of the Charge States

If instead of coming from similar ions, line radiation from dissimilar charge species is measured, the relative densities of these unlike charge states may be found. The cold-electron temperature, being known, can be used to evaluate $S_x(\epsilon)$ for every transition. Solving Equation (III-21) for n_0 , the ratio of densities of charge q to charge k, after correcting the intensities for transmission differences, is:

$$\frac{n_q}{n_k} = \frac{I_q A_k S_k \sum A_q}{I_k A_q S_q \sum A_k} \quad , \quad (\text{III-23})$$

where the notation is the same except that the original subscripts are

suppressed in order to show only the ionic charge, q or k . Denoting the total particle density by n_T , we have:

$$n_T = \sum_{k=0}^Z n_k \quad . \quad (\text{III-24})$$

If this relation is divided by n_0 , the density of neutral neon, all of the quantities on the right are known spectroscopically via Equation (III-23), and the left side is:

$$\frac{1}{F_0} = \frac{n_T}{n_0} \quad , \quad (\text{III-25})$$

in which F_0 is the fraction of the total particle density composed of neutral neon. Now, of course, the fractional population densities of other states follow from:

$$F_k = \frac{n_k}{n_0} F_0 \quad . \quad (\text{III-26})$$

Ideally, the absolute densities are discovered next by using the result of kinetic theory:

$$P = n_T k_B T \quad , \quad (\text{III-27})$$

where P is the corrected pressure [see Equation (II-1)] and T the temperature in the ionization gauge in degrees Kelvin.

The Electron Density

Once n_T is multiplied by the various F_k 's to give the densities of the different charge states, the assumption of uniform densities throughout the microwave cavity is used to get the electron density, n_e . Equation (II-2) is divided by the plasma (cavity) volume to yield

the relationship needed:

$$n_e = \sum_{k=1}^Z k n_k \quad . \quad (\text{III-28})$$

This represents all electrons in the plasma--both cold and hot. Thus, as implied by Equation (III-12),

$$n_e = n_C + n_H = n_C(1 + \epsilon) \quad . \quad (\text{III-29})$$

C. THE IONIZATION MODEL

Already a way has been pointed out to find some important intrinsic plasma parameters through an excitation model and the experimentally observed line intensities. Now we turn to the theoretical ionization model in order to extend our understanding further.

Methods of Ionization and Model Reduction

There are nearly as many ways to ionize as to excite the atomic system. These are atom-photon, atom-atom, and atom-electron interactions which supply the energy necessary to free an orbital electron from the field of the nucleus. Fortunately, the overlap between ionization and excitation processes is great; much of the work for formulating a model has been done in the preceding pages.

As noted before, the plasma is assumed to be thin to high-energy photons so that though they have the energy to ionize, they escape the plasma first. It is for this reason that the ELMO facility is surrounded by a three-inch lead wall.

In addition, atom-atom collisions are still considered negligible on account of the low ion temperature. The creating of an ion of a

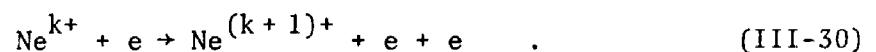
particular charge by charge exchange (not symmetrical resonance charge exchange) has been handled earlier. Analogous to the excitation model, it is assumed that the charge-exchange rates for non-symmetrical encounters are small compared to electron-impact ionization rates.

The dominant ionization mechanism then is atom-electron collisions. As dictated by the corona model, the atom begins in the ground state. As will be discussed later, atom-electron impact results in two distinct modes of ionization. Denoting by Δk the change in charge during the collision, these are: (1) single-step ionization for which $\Delta k = 1$, and (2) multi-step ionization for which $\Delta k > 1$. Both of these will be included in the ionization model.

These are the ways in which ions are formed. Ions of a particular charge are lost from the system also. Obviously a single electron impact does not preclude additional collisional ionization which effects a decrease in the population of the parent ion. The populations of ions having a high enough charge may be depleted by recombination as in Equation (III-9). Usually this may be ignored as can be non-symmetrical charge exchange which also replaces a highly charged ion by two lower-charge-state ones. Perhaps the dominant means of decay of ionic populations is simply leakage into the loss cone. This is the factor which limits the degree of ionization a particle sustains--its time in the plasma.

Electron-Impact Ionization Modes

Attention is focused first on the single-step process in which a single electron is stripped from the atomic system:



The required energy is simply the ionization energy of Ne^{k+} . These are given in Table 1. The hot (20 keV) electrons clearly may take part in this ionization mode; the cold electrons will partake to an extent dependent on their temperature and on which ions are to be formed.

Table 1. Ionization Energies for Different Neon Ions*

Atomic System	Ionization Energy in eV
Ne (neutral)	21.56
Ne^{1+}	41.07
Ne^{2+}	63.5
Ne^{3+}	97.02
Ne^{4+}	126.3
Ne^{5+}	157.9
Ne^{6+}	207.2
Ne^{7+}	239

*Reference 100.

As was done in Equation (III-11), the ionization rate may be divided into two parts for the two temperature groups:

$$S_k^{k+1}(\epsilon) = S_k^{k+1}(C) + \epsilon S_k^{k+1}(H) \quad . \quad (\text{III-31})$$

Lotz gives these rates in tabular form⁶⁸ for Maxwellian distributions of electrons with temperatures below 1000 eV. Knowing the cold-electron temperature, we may interpolate his data to calculate $S_k^{k+1}(C)$. In a later paper,⁶⁹ he gives the single-step ionization cross sections for electrons

with energy E as:

$$\sigma_k^{k+1} = \sum_i a_i q_i \frac{\ln(E/P_i)}{E P_i} \left[1 - b_i Y_i(E) \right] \quad (\text{III-32})$$

where

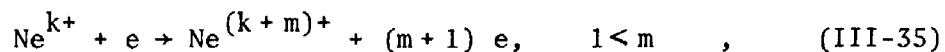
$$Y_i(E) = \exp \left[-c_i \left(E/P_i - 1 \right) \right] \quad (\text{III-33})$$

In these equations q_i is the number of equivalent electrons in the i th subshell, P_i their binding energy,⁷⁰ and a_i , b_i , and c_i are constants in the sum over all subshells (given in the text). Following the example of Equation (III-18),

$$S_k^{k+1}(H) = v \sigma_k^{k+1} \quad , \quad (\text{III-34})$$

where v is the velocity of 20 keV electrons.

Ionization by the multi-step mode,



is executed chiefly by the hot electrons. Experiments by Stuber⁷¹ indicate that cold electrons (tens of eV) have a low probability of initiating such events.

The manner in which multi-step ionization is achieved comprises of two possible actions: Auger processes and electron shake-off. An Auger process⁷² occurs following the removal of an inner-shell electron from a system (by electron impact for instance). As an outer-shell electron realigns itself to fill the vacancy, the corresponding difference in the binding energy, ΔE , can liberate a second orbital electron giving it a kinetic energy⁷³:

$$T_A = \Delta E - P_A \quad , \quad (\text{III-36})$$

where P_A is the binding energy of the Auger electron. Here we have $\Delta k = 2$. For a K-shell vacancy in neon, T_A may exceed 800 eV.^{74,75} An Auger electron with so great an energy could instigate another Auger event by knocking out an L-shell electron. A sequence like this has $\Delta k = 4$.

The electron shake-off phenomenon⁷⁶ follows a sudden change in the electric potential of a nucleus screened by the inner shells of electrons as seen by a loosely bound electron. This sudden change (a K- or L-shell ionization) takes place more rapidly than the orbital electrons can adjust to it; hence, the shaking off of these electrons may occur, and $\Delta k > 1$.

How the initial vacancy was created does not seem to matter, nor does where it occurs matter.⁷⁷ Carlson has found⁷⁸ that low energy X-rays, capable only of outer shell ionization, can produce multi-ionized neon. The effect of an inner shell electron vacancy should be even greater because the inner shell orbit should be a more efficient shield of the nuclear charge.

Shake-off may occur with or without an Auger process. It is distinguished from the Auger effect by its relation to multi-step ionization during beta decay^{79,80} in which the charge change of the nucleus replaces the creation of an electron-shell vacancy. Coupled together, Auger ionization and shake-off may account for rather large values of Δk for a single atom-electron collision. Table 2 gives the charge spectra resulting from a K- or L-shell vacancy in neon as measured by Carlson, Hunt, and Krause.⁸¹

Table 2. Charge Spectra Resulting From a K- or L-Shell Vacancy in Neutral Neon*

Ionic State	K-Shell Vacancy	L-Shell Vacancy
Ne ¹⁺	1.0%	87.3%
Ne ²⁺	73.6%	11.9%
Ne ³⁺	22.0%	0.8%
Ne ⁴⁺	3.1%
Ne ⁵⁺	0.3%
Ne ⁶⁺
	100%	100%

* Reference 81.

Process (III-35) may take place for $k = 0, 1, 2, \dots$ so long as the incoming electron is sufficiently energetic. Unfortunately, the appropriate cross sections are not available except for $k = 0$. These are given in an experiment by van der Weil and others⁸² as:

$$\sigma_0^i = \frac{4\pi a_B^2 E_H}{E} \left[M_i^2 \ln \left(E/E_H \right) + C_i \right], \quad (\text{III-37})$$

in which M_i and C_i are empirical constants for a $\Delta k = i$ ionization.

The rates for multi-step ionization are then:

$$S_0^i(H) = v \sigma_0^i, \quad (\text{III-38})$$

where again the assumption is made that $v \sigma_0^i$ is approximately constant over the hot-electron distribution.

The Ion Population Equations

The ionization model, to repeat for emphasis, consists of electron collisions with ground state atoms leading to both $\Delta k = 1$ and $\Delta k > 1$ events. All other varieties of ionization are disregarded. Recombinations and charge exchange are neglected.

Consider the plasma to be in equilibrium with its electron population. Let the populations of ionic charge states (which are constant in time) be N_0 for neutral neon, N_1 for Ne^{1+} , N_2 for Ne^{2+} , etc. The total population is

$$N = \sum_{k=0}^{10} N_k \quad . \quad (\text{III-39})$$

Note that impurities are not considered.

Introduce into the plasma an assembly of n neutral atoms at time $t = 0$. Assume that n is much smaller than N so that this process is a small perturbation on the plasma. Ionization begins on the neutral assembly as a result of the plasma electrons--both the hot and the cold temperature groups. Represent the populations of charge states within the assembly by $n_0(t)$, $n_1(t)$, $n_2(t)$, etc. As a first approximation, assume perfect confinement:

$$n = \sum_{k=0}^{10} n_k(t) = \text{constant} \quad . \quad (\text{III-40})$$

The initial condition placed on the $n_k(t)$'s is:

$$n_k(0) = n \delta_{0,k} \quad . \quad (\text{III-41})$$

After a time, τ_c , the $n_k(t)$'s approach the plasma equilibrium

concentration such that:

$$\frac{n_k(\tau_c)}{n} \sim \frac{N_k}{N} \quad . \quad (\text{III-42})$$

At this time, losses from the $n_k(t)$'s must be considered. The assumption of perfect confinement otherwise leads to

$$n_k(t) = n \delta_{10,k} \quad , \quad (\text{III-43})$$

for t large enough. In actuality, the higher charge states are depleted by drifts out of the plasma, wall recombinations, etc. The lower charge states are replenished by a continuous supply of neutrals flowing into the plasma. Were these effects included, the time derivatives of the $n_k(t)$'s must vanish at $t = \tau_c$.

In the absence of losses and the input of new gas, τ_c may be thought of as a particle confinement time--a measure of how long a neutral assembly of gas entering the plasma must be contained in order to reach the equilibrium of ionic concentrations. The differential equation governing $n_0(t)$ is:

$$\frac{dn_0}{dt} = -n_c \left[S_0^1(\text{C}) + \epsilon S_0^T(\text{H}) \right] n_0 \quad . \quad (\text{III-44})$$

The first term on the right is single-step ionization of neutrals due to cold electrons of density n_c ; the second term is the loss rate of neutrals by both ionization modes caused by hot electrons [Equation (III-12)]:

$$S_0^T(\text{H}) = S_0^1(\text{H}) + S_0^2(\text{H}) + S_0^3(\text{H}) + \dots \quad (\text{III-45})$$

For the i th ionization state, the differential equation is

$$\frac{1}{n_C} \frac{dn_i}{dt} = - S_i^{i+1}(\epsilon) n_i + S_{i-1}^i(\epsilon) n_{i-1} + \epsilon S_0^i(H) n_0 (1 - \delta_{1,i}). \quad (\text{III-46})$$

[The $S(\epsilon)$'s are given by Equation (III-31).] The last term on the right is the contribution due to multi-step ionization. Note that if $i = 1$, there is none. As can be seen in Equation (III-46), this mode is taken into account only if the initial state is a neutral atom. This concludes formulation of the ionization model and its population balance equations.

D. PLASMA INFORMATION FROM THE IONIZATION MODEL

Using the ionization formulas of the above subsection, the set of first-order differential equations for the $n_k(t)$'s may be solved in a straightforward if tedious manner for any value of ϵ . This allows us to deduce even more of the intrinsic plasma variables.

Ion Containment and Temperature

After the fashion of Equations (III-24), (III-25), and (III-26), the time history of the fractional population densities may be calculated by a computer. These have presumably already been determined by experiment; therefore a comparison specifies τ_c , and the particle confinement time is known. The mean lifetime of a neutral before ionization follows from Equation (III-44) [cf. Equation (III-3)]:

$$t_{M\ell} = \frac{1}{n_C \left[S_0^1(C) + \epsilon S_0^T(H) \right]}. \quad (\text{III-47})$$

A comparison of τ_c and $t_{M\ell}$ gives an idea of the duration of ion heating

by electron impact. Then Equation (II-3) may be used to approximate T_i , the ion temperature in the neon plasma.

The Role of the Hot Electrons

The parameter, ϵ , if it could be estimated by experimental observations, will tell the densities of the cold and hot electrons. Afterwards, the relative importance of each for the excitation and ionization models could be determined. By setting $S_0^k(H) = 0$ for $k \geq 2$, one turns off the multi-step ionization mode. By this technique, the part which that mode plays in populating ionic states is learned.

IV. EXPERIMENTAL CONSIDERATIONS

This section contains a survey of all experimental work done for this thesis. Included are equipment descriptions and conditions for use.

A. THE VACUUM ULTRAVIOLET SPECTROMETER

The manipulation of XUV photons requires special care. At wavelengths below 2000 Å, they are absorbed by air, especially oxygen. Below 1040 Å, all known lens and window materials cease to be transparent. Finally, near 300 Å, the reflection coefficient of diffraction gratings becomes low except at grazing incidence.⁸³ The spectrometer utilized in the present research meets all of the requirements for transmission in the XUV.

Description

The vacuum ultraviolet spectrometer which served during the experiment is the McPherson Instrument Corporation's Model 247 grazing incidence monochromator spectrograph. This spectrometer was used as a scanning monochromator to measure the intensity of spectral lines transmitted from the plasma. It conforms optically to a Rowland circle of diameter 2.2 meters.⁸⁴ This means that the reflection grating is concave with a radius of curvature equal to the circle diameter and that the center of the grating is tangent to the circle. Such an arrangement has the property that a source illuminating a point on the circumference of the circle will have its spectrum focused on the circle⁸⁵ as in Figure 9. The Rowland circle is thus defined by the entrance slit, the grating, and

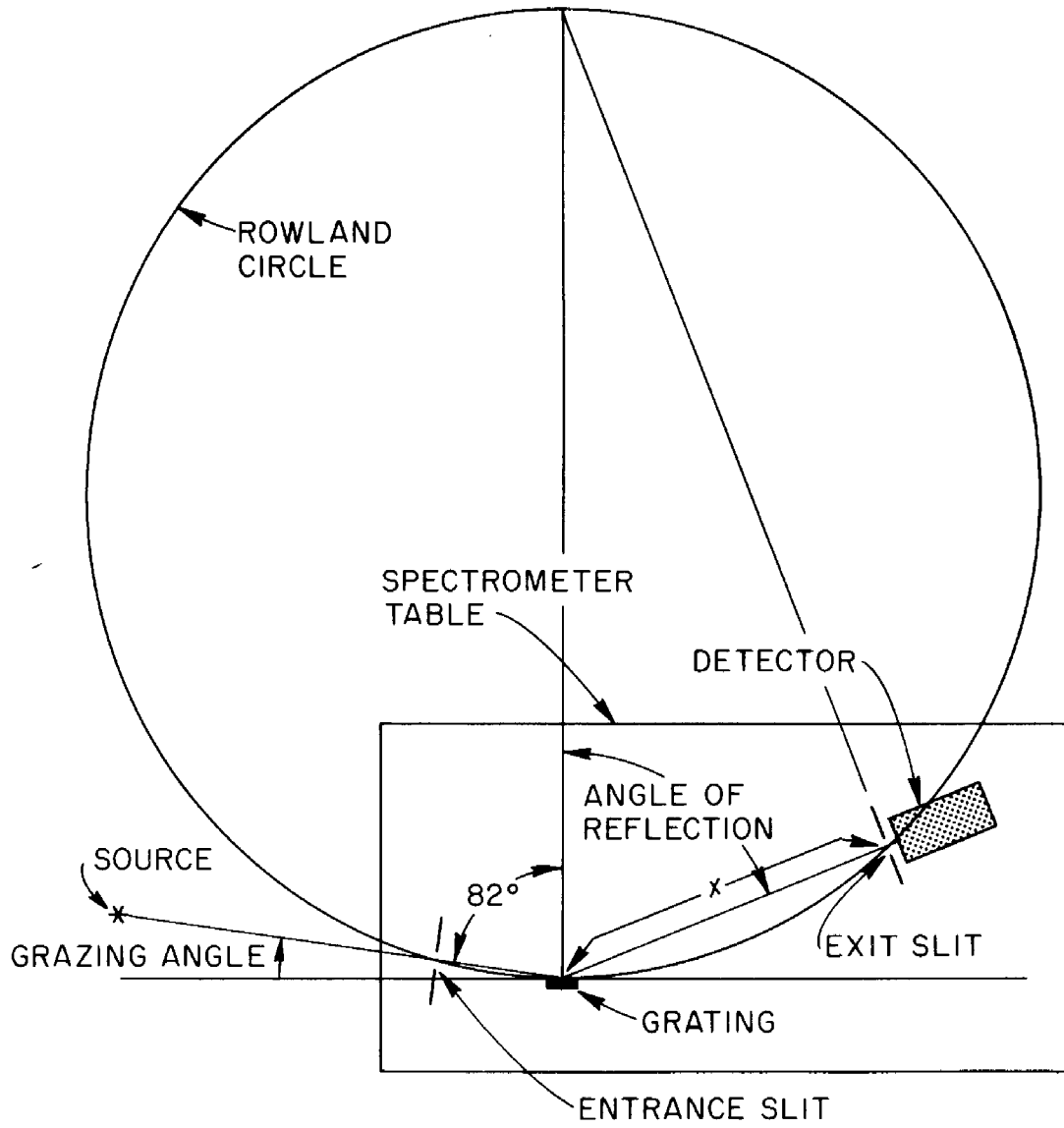


Figure 9. The Rowland Circle Spectrometer Configuration.

the exit slit. The entrance slit is fixed for this experiment so that the angle of incidence is 82° . The approximate wavelength of radiation at the exit slit is given by the grating equation⁸⁶:

$$m\lambda = d \left[\sin 82^\circ - \sqrt{1 - \left(\frac{x}{87.282} \right)^2} \right] , \quad (\text{IV-1})$$

where m is the order, λ the wavelength, d the distance between rulings on the grating, and x the reading of a counter on the spectrometer which tells the distance of the exit slit from the grating in inches. The quantity under the radical is the square of the sine of the angle of reflection.

The entrance and exit slits of the spectrometer are effectively 1 cm in height with a variable width. As much as possible, the slit separation remained the same throughout the experiment, but since line intensities varied over four orders of magnitude, a second slit width was necessary. Weak lines could not be detected with the narrow slit setting, and strong lines saturated the detector at the wider setting. The two widths selected are nominally 20 and 30 microns though a sixteen or seventeen micron zero off-set is suspected; thus, the widths are perhaps 4 and 14 microns instead. Several lines could be measured at both slit openings. The multiplication factor between intensities at the two settings was a constant and was used to convert all intensities to what they would have been at the same slit width. Both entrance and exit slits were set on the same setting for each measurement.

The grating employed is supplied by McPherson Instrument Corporation: catalog number 35-52-47-020. There are 300 grooves per millimeter on the 52 by 30 millimeter ruled, concave surface. The total number of

grooves, N , is 300×52 or 15,600. The resolving power, RP , is given as⁸⁷:

$$RP = mN = \lambda/\Delta\lambda \quad , \quad (IV-2)$$

where $\Delta\lambda$ is the separation between two lines of similar intensity which can barely be resolved by the grating. The McPherson grating is rated⁸⁸ at 80% of its theoretical resolving power; therefore, RP for the first order spectra is approximately 12,500 in practice. Another feature of the grating is its special gold coating. The electron density of gold and the angle of incidence used in theory⁸⁹ cause total reflection at wavelengths greater than 22 Å.

Vacuum in the instrument is maintained at approximately 10^{-6} Torr by its own pumping system. This system consists of a mechanical roughing pump and a diffusion pump. In the foreline between pumps is a molecular sieve trap. Between the main spectrometer chamber and the diffusion pump is a liquid nitrogen cold trap.

Mounting

The problem in mounting the 1400 point spectrometer⁹⁰ is to align the plasma, the entrance slit, and the grating and to observe the plasma along a midplane diameter. The geometry of ELMO required a horizontal optical axis about five and a half feet above floor level. The distance from the plasma to the entrance slit was close to eleven feet.

Though the spectrometer has leveling screws in its legs, the optical axis was above their maximum extension. A forklift was used to raise the spectrometer to a platform 14 inches high from which the leveling screws could be used.

Once the instrument was in the right neighborhood, a laser beam was employed to optimize alignment. The beam was directed through the microwave shield of the plasma cavity to serve as an optical axis. It was then a simple matter to position the spectrometer so that the beam passed through the entrance and exit slits with the latter placed in the usual location of the central image.

The gap between ELMO and the entrance slit was bridged by a one-inch-diameter brass tube constrained at both ends by quick-connect vacuum fittings. This allowed for flexibility and a minimum load on the entrance slit carriage of the spectrometer.

The brass tube passed through a two-inch hole in the three-inch-thick lead shield which surrounds the ELMO facility. The grating, which was now situated in line of sight with the position of the plasma line radiation, was also in line of sight with the plasma bremsstrahlung emission. If this radiation was also in line of sight of the detector, the background noise from the detector would be large. Note that "line of sight" for X-rays has a different meaning than "line of sight" for XUV photons. The structure of the spectrometer, vacuum walls, slits, etc., are essentially transparent to hard X-rays. The reason that motivated using the largest grazing angle possible was so that as much of the domain of the detector as possible could be in the shadow of the three-inch lead wall. The detector was separated from the exit slit by a quarter-inch lead plate for additional protection.

B. THE DETECTOR

The monochromatic line radiation from the exit slit of the spectrometer is now ready for detection. This is done by a channel electron multiplier (CEM). From it a signal is relayed through a pulse counting circuit and an integrator to a strip chart recorder. Hence, the relative number of photons of a particular wavelength per second incident on the CEM is given.

Description of the CEM

The actual detector used is a Mullard, Inc., model B419BL. It consists of a planar spiral of hollow lead glass tubing 2.2 mm in diameter and about 10 cm long. The outside end opens into a cone-shaped "photon catcher" of 0.9 cm diameter. The opposite end, the output end, is closed. Inside the tube and cone is a high resistance material which emits a photoelectron when struck by an ultraviolet photon. If a high potential difference is applied across the length of the CEM with the output end positive with respect to the input end, the photoelectron is accelerated down the tube and creates secondary electrons upon impact with the wall. These continue the multiplication process as they progress toward the output. For high enough voltage, the gain saturates at around 10^8 . This means that in the gain saturation mode, a single photon incident on the detector input results in a pulse of 10^8 electrons at the terminal end.⁹¹

Ray and Barnett have found⁹² that the effective area of the cone is increased if a wire grid is placed immediately before the opening of

the cone with both at the same potential. This was done in the present experiment. The voltage applied to grid and cone was -3200 V while the output was terminated with a megohm resistor to ground. This was sufficient for gain saturation.

The response of a CEM makes it a good detector for XUV photons. The sensitivity is generally uniform up to 1200 \AA at which point it begins to decrease rather rapidly. At 1500 \AA , the CEM is unresponsive.⁹³ Two other features are the excellent stability of the CEM signal and the very low background noise -- on the order of a count a minute.

Circuitry

After the burst of electrons comes to the back end of the CEM, it enters the circuit shown in the block diagram of Figure 10. The preamplifier is the ORTEC model 113 scintillation preamplifier powered by the ORTEC model 115 power supply. Next is a linear amplifier by Tennelec, model TC203BLR. Further pulse shaping and pulse discrimination is accomplished by an ORTEC model 408 bias amplifier. At this point, the output branches.

One choice is an ORTEC model 441 ratemeter which integrates the pulses over selected periods of time and hence wavelength according to the scan speed of the spectrometer. In this experiment the output of the ratemeter was fed into a strip-chart recorder. The second branch consists of a pair of ORTEC model 431 timer-scalars. One of these acted as a scalar to count the number of pulses from the CEM. The other could be used as a timer in a master-slave relationship with the scalar to determine the number of counts in a particular time interval.

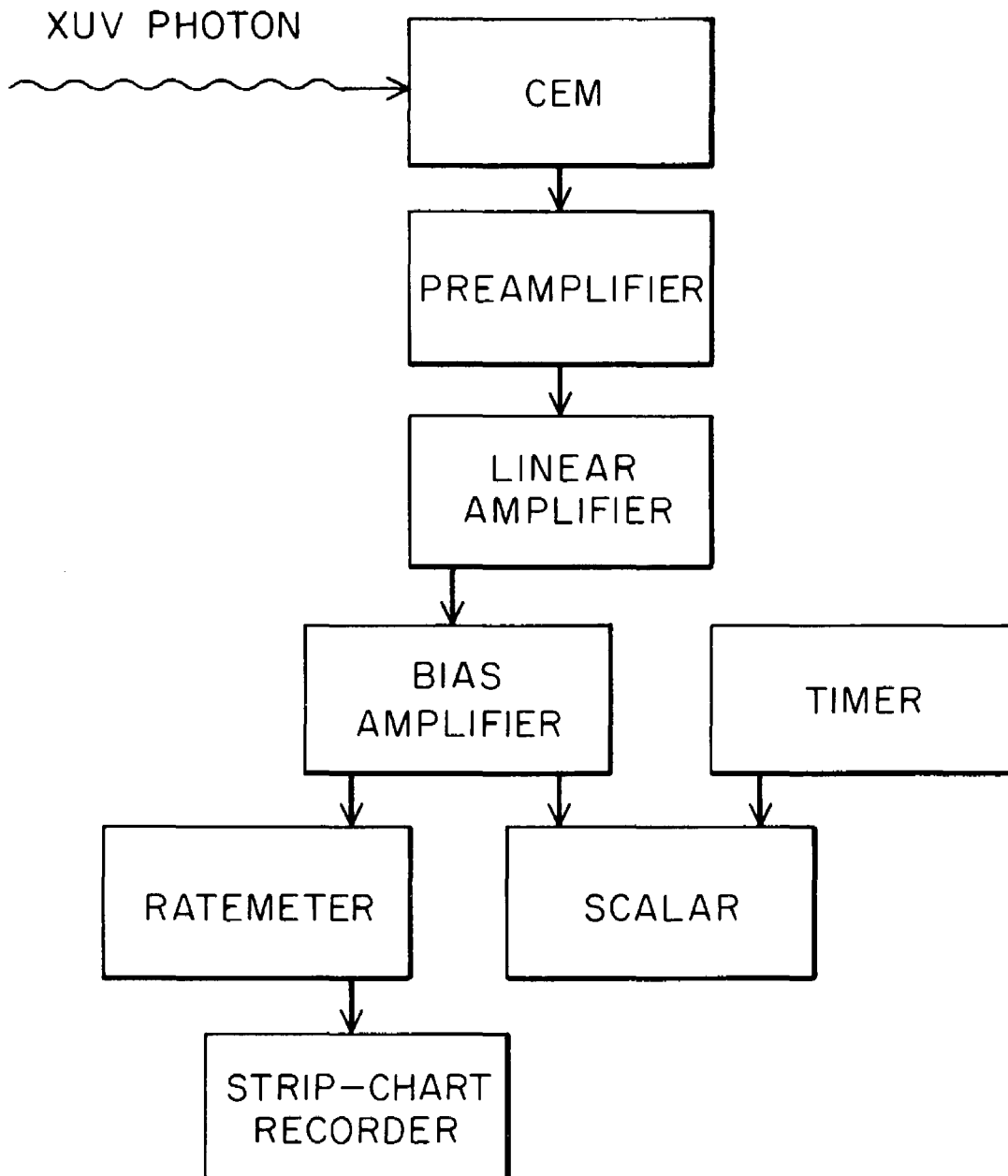


Figure 10. A Block Diagram of the Detector System.

All of these instruments except the preamplifier, its power supply, and the strip chart fit into a NIM-Bin with the usual power supply.

C. CALIBRATION

The calibration of the instrument involved two separate quantities: wavelength and intensity. The first is very easy; the second very difficult without special care.

Wavelength Calibration

Three things combine to make this phase of the calibration very simple. These are (1) Equation (IV-1), (2) a wavelength marker, built in the spectrometer, which sends a pulse to a second pen on the strip-chart recorder for every one-hundredth of an inch of travel of the exit slit along the Rowland circle, and (3) a listing of spectral lines compiled in order of increasing or decreasing wavelength.^{94,95} The difference between calculations from formula (IV-1) and the tabulated values of lines increases from 0.5 Å to 3 Å as λ goes from 200 Å to 1300 Å. Most of this is probably due to a slight zero offset of the scale. In any event, the cure is to draw an experimental spectrum on a one-dimensional graph. When this is compared to a similar graph of tabulated lines, the identification is nearly trivial.

Intensity Calibration

What is desired from an intensity calibration is the sensitivity, $S(\lambda)$, of the spectrometer-detector system to a given photon intensity as a function of λ . A working definition of sensitivity is:

$$S(\lambda) = \frac{R(\lambda)}{X I(\lambda)} \quad , \quad (\text{IV-3})$$

where $R(\lambda)$ is the system response in some convenient unit (e.g., counts/sec or nanoamperes) to a known intensity of light, $I(\lambda)$, given in photons/cm² sec. X is the effective slit area. Since there is no standard of ultraviolet emission, $I(\lambda)$ must be obtained indirectly.

This problem is dealt with by the branching ratio technique.⁹⁶ The idea here is to pick a set of atomic energy levels which decay with well known transition probabilities by emission of either an ultraviolet or a visible photon. Table 3 lists pairs of such lines, the intensities of which are related by the ratio of the transition probabilities:

$$\frac{I_{uv}}{I_{vis}} = \frac{A_{uv}}{A_{vis}} \quad (IV-4)$$

Given a calibrated visible spectrometer, the sensitivity of the ultraviolet instrument is calculated by:

$$S_{uv}(\lambda_{uv}) = \frac{R_{uv}(\lambda_{uv})}{R_{vis}(\lambda_{vis})} \cdot \frac{X_{vis}}{X_{uv}} \cdot \frac{A_{vis}}{A_{uv}} \cdot S_{vis}(\lambda_{vis}) \quad (IV-5)$$

The visible spectrometer used for this calibration is a half meter Jarrell-Ash, the sensitivity of which is procured with a calibrated tungsten light source via Equation (IV-3).

It is important that both spectrometers see the same volume of plasma through the same solid angle and from the same distance so that Equation (IV-4) holds. A special "T" was installed in the vacuum line between the light source and the entrance slit of the McPherson. It contained a front-surface mirror on a pivot which could be adjusted to reflect the source light through a window at the base of the T into the entrance slit of the visible spectrometer. With the mirror rotated out

Table 3. Line Pairs* Used in the Branching Ratio Calibration

Atomic Specie	λ_{uv}	λ_{vis}	A_{uv}/A_{vis}
H I	1026 Å	6563 Å	1.26
H I	973	4861	1.52
H I	950	4340	1.63
He I	537	5016	42.3
He I	522	3964	34.8
He I	515	3614	34.1
He II	243	4686	1.42
He II	237	3203	1.87

*Reference 96.

of the way, the source light passed unobstructed through the T to the XUV instrument. In this way the optical path lengths for both spectrometers can be made the same.

Nevertheless, the presence of the front-surface mirror and the window in the vacuum line must be taken into account. Table 4 lists the sensitivity of the Jarrell-Ash corrected for the presence of the mirror and window. The detector is a photomultiplier tube driven by -700 V. The spectrometer slits are 1.5 cm by 50 microns.

The untimely shutdown of the ELMO experiment necessitated an alternate light source for the branching ratio measurement. (The neon data were previously collected.) Chosen for this was ORNL's INTEREM facility which, like ELMO, heats electrons by ECH but in a mirror-quadrupole field.⁹⁷

Table 4. Sensitivity Versus Wavelength for the Jarrell-Ash Visible Spectrometer

λ	$S(\lambda)$	
6563 Å	5.24×10^{-10}	<u>nanoamperes</u> photon/sec
5016	1.28×10^{-7}	
4861	1.50×10^{-7}	
4686	1.83×10^{-7}	
4340	2.28×10^{-7}	
3964	2.61×10^{-7}	
3614	2.61×10^{-7}	
3203	3.05×10^{-7}	

Table 5 shows the detector responses to the line pairs listed in Table 3. Assuming the time-independence of the plasma, a series of measurements were taken with one spectrometer, and then the other by adjusting the mirror. Approximately a 10% error in readjusting the mirror for measurements at a different pressure was possible. These data were taken in INTEREM at microwave power levels of 100, 200, 300, 500, and 1000 watts. The ratio of responses, R_{uv}/R_{vis} , generally is insensitive to power level. Pressures were selected to maximize system response while minimizing self-absorption of the resonance UV lines. It is found that the quantity R_{uv}/R_{vis} increases as pressure is reduced if self-absorption is a problem. For pressures as low as 10^{-6} Torr, He I lines show this effect to some extent because the entire optical path (about ten feet) is occupied by

ground state atomic helium. On the other hand, helium ions exist only in the microwave cavity, and He II lines are not affected. Similarly, atomic hydrogen dwells only in the plasma while the rest of the optical path is filled by H₂. More will be said later on how this affects the assumption that the plasma is optically thin.

Table 5. Average Ratios of Spectrometer Responses to Calibration Line Pairs

Atomic Specie	λ_{uv}	λ_{vis}	R_{uv}/R_{vis}
H I	1026 Å	6563 Å	16420 $\frac{\text{counts/sec}}{\text{nanoampere}}$
H I	973	4861	80.6
H I	950	4340	68.3
He I	537	5016	2112
He I	522	3964	1750
He I	515	3614	1786
He II	243	4686	247
He II	237	3203	186

Because the slit area of the McPherson is not precisely known, only a relative intensity calibration is possible. Figure 11 shows the results of the sensitivity calibration normalized so that $S(237 \text{ Å}) = 1.00$. A least-squares fit for a straight line is taken as the sensitivity. The He I points lie somewhat low, particularly He I 537 (which is not included in the least-squares fit), probably due to resonance absorption. The

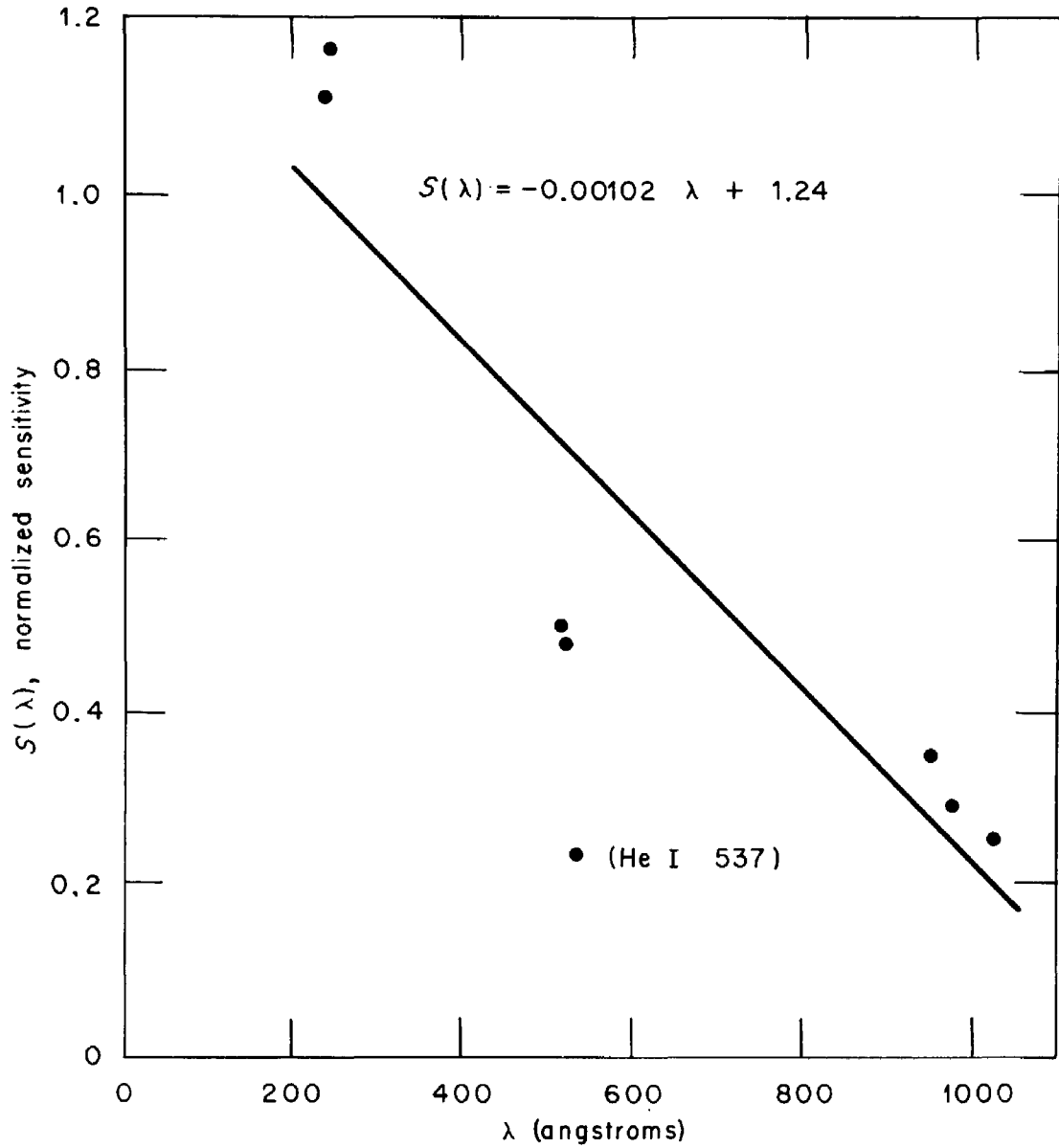


Figure 11. Normalized Sensitivity of the XUV Spectrometer versus Wavelength--The Least Squares Fit to a Straight Line Omits the He I 537 Data Point.

straight-line-response assumption leads to a normalized sensitivity:

$$S(\lambda) = - 0.00102 \lambda + 1.24 \quad , \quad (\text{IV-6})$$

for which λ is given in angstroms.

D. OUTPUT

As mentioned, the spectrometer output is a time-integrated (wavelength-integrated) signal recorded on a strip chart. Described here is the nature of the output signal.

Signal Amplitude

Counting rates useful for measurements fell between the values of 2 or 3 counts/sec, where continuum radiation was the limiting factor, and about 3500 counts/sec at which point CEM saturation begins. A check with a variable frequency pulse generator showed that ratemeter output to the strip chart was linear with frequency for all counting scales used.

Typically, scans were taken at 0.01 or 0.02 in./min so that the time constant of the ratemeter did not distort the line profile. Figure 12 shows relative amplitudes of components of the $^3P-^3P^o$ multiplet⁹⁸ of Ne III 489 taken at a scan speed of 0.02 in./min with the narrow slit setting. The intensity scale is roughly 11 counts/sec per inch. The results of a comparison between experimental and theoretical⁹⁹ component intensities is very good and is given in Table 6.

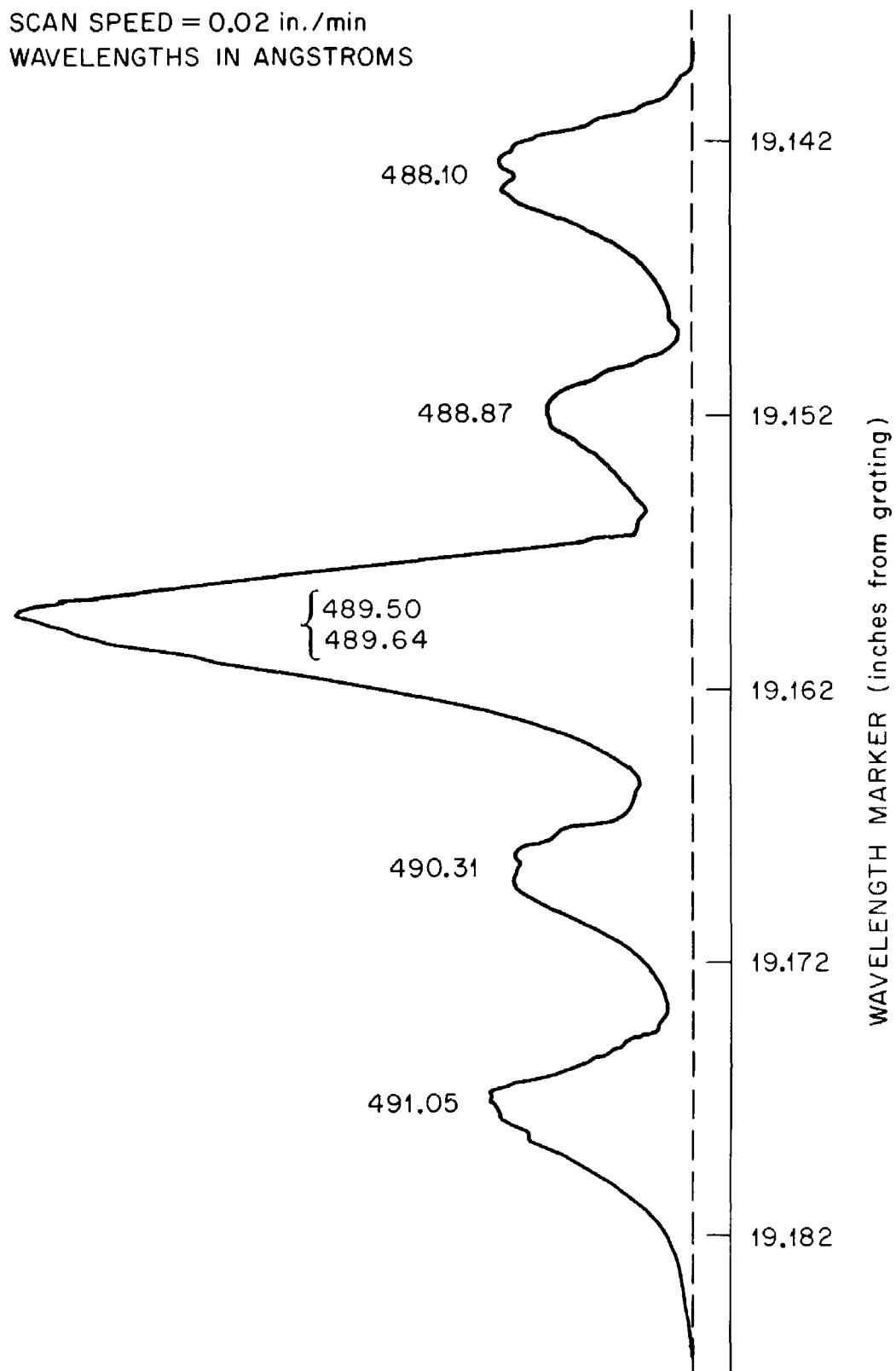


Figure 12. Strip Chart Trace of the Ne III 489 Multiplet.

Table 6. Relative Intensities of the Multiplet Components of Ne III 489 as Percentages of the Total Multiplet Strength

λ	Theoretical*	Experimental
488.10 Å	13.9%	14.1%
488.87	11.1	10.3
489.50	41.7	48.1 (blend)
489.64	8.3	
490.31	11.1	13.0
491.05	13.9	14.5
	100%	100%

* Reference 61, pp. 54, 55.

Dispersion and Resolution

The dispersion of the McPherson spectrometer is a function of x , the chord length across the Rowland circle between the grating and the exit slit. By differentiating Equation (IV-1) with respect to x , one derives the first-order dispersion or the reciprocal plate factor, PF:

$$\frac{d\lambda}{dx} = (\text{PF})^{-1} = \frac{x}{87.282} \frac{d}{dx} [(87.282)^2 - x^2]^{-\frac{1}{2}}, \quad (\text{IV-7})$$

where x is given in inches, and the slit separation, d , is 3.33×10^4 Å. Thus, the wavelength spread between markers (0.01 inch) on Figure 12 where $x = 19.142$ is 0.86 Å.

Using this result, it is easily seen that the full width at half maximum (FWHM) is on the order of 0.3 Å for any of the Ne III components

with the narrow slit setting. This instrument width represents a limit on the resolution to be expected; for example, the 489.50 and the 489.64 components, separated by 0.14 Å were not resolved. In the course of this investigation, the nearest neighbors which could be resolved were Ne II 446.25 and Ne II 446.59 which are 0.34 Å apart--about the same as FWHM. Note that in Equation (IV-2) with $\lambda = 489$, one finds for $\Delta\lambda$, the least distance between resolvable lines, a value of 0.04 Å, considerably less than the practical limit. This suggests that the slits rather than the grating are responsible for the limit of resolution.

V. OBSERVATIONS AND MEASUREMENTS

In this section is a summary of all experimental observations. The theory of Section III is applied, and the intrinsic plasma parameters are calculated.

A. GENERAL OBSERVATIONS

Well over 200 lines of various elements were detected in scans over many wavelength intervals. The lines ranged from a short wavelength of 204 Å to the longest first order wavelength at 1215 Å. Up to the fourth order of several lines was observed. The charge state of the parent atomic system varied from neutral to six times ionized. Below is a survey of line identification, impurities, charge states discovered, and the neon data relevant for this thesis.

Line Identification

Of the lines detected, about 90% were positively determined. The technique for identification has been described in Section IV, C. There are two factors which can make the identification difficult.

The first of these is the blending or overlap of lines. The presence of a weak line was uncertain if it lay near any other line of any order of any atomic system. Under special conditions there is some relief from this problem. If the interfering line is an impurity, sometimes its intensity will decrease over a long period of operation, which then leaves the line of interest alone. Also, the expected contribution to the blended lines by the impurity may often be judged by the strength

of impurity peaks of the same kind which lie nearby. Then the other line's intensity may be estimated. A second help is available if the weak line is not too weak and not too close to the intruder. Now what one does it to attempt to resolve the lines in the second order at twice the wavelength. The separation between lines in the second order is almost double, which makes resolution easier. (The actual change in the separation is dictated by the dispersion.)

The second difficulty has no solution; it is the appearance of a line for which there is no listing in tables. One particular instance of this stands out in the neon scans. The Ne V 482 multiplet seemingly had been detected though the intensities of multiplet components did not follow theoretical predictions--one component was completely absent--and there was an apparent quarter-Angstrom red shift. Impurities were ruled out, but the explanation was an unidentifiable cluster of lines which appeared in first order at 241 \AA .

Impurities

Though neon was the only gas for which a complete set of data was taken before the shutdown, others were used for short terms as the feed gas. After changing the feed gas, an hour or more of operation was required before all evidence of the previous feed gas was gone. More important, certain impurities persisted throughout the experiment. Notable among these was Al III 560.4, which was due to the sputtering of aluminum from the cavity walls. This line was weak relative to the neon lines, yet not as dim as the other pollutants, carbon and oxygen, which were very weak, generally less than five counts per second.

Charge States

Depending on the feed gas, different degrees of ionization were observed. Four-times ionized neon, three-times ionized nitrogen, and six-times ionized argon were unambiguously detected with each as the respective feed gas. In addition, for neon and nitrogen the next higher charge states, Ne VI and N V, showed some evidence of being present though not enough to say so without doubt.

The Neon Data

On the order of 80 lines equally divided among Ne I, Ne II, Ne III, and Ne IV were recorded during neon operation. Besides these were three Ne V lines and the aforementioned five-times ionized line, Ne VI 402. Unfortunately, this is not all usable data. For example, National Bureau of Standards tables¹⁰⁰ of transition probabilities, the A_{ik} 's, list only a couple of lines each for Ne I and Ne II. Without this vital information, the intensity of a line is little comfort.

For each of the ionized states, the most intense transitions have been chosen for the actual calculations of Section III with the necessary atomic data taken from the NBS tables. For neutral neon, Lawrence and Liszt¹⁰¹ give the lifetimes, τ^* , and oscillator strengths, f , of several resonance lines. Then, using Equation (III-2) and

$$A_{ik} = \frac{6.67 \times 10^{15}}{\lambda^2} \frac{(2 J_i + 1)}{(2 J_k + 1)} f \quad , \quad (V-1)$$

the transition probabilities may be calculated.¹⁰² In this formula, λ is given in Angstroms while J_k and J_i are the initial and final angular momentum states (1 and 0 for the transitions selected). The shortest

possible wavelengths were selected to minimize the cascade feeding. Table 7 lists transitions employed for this dissertation. The relative intensities are derived from Equation (IV-3) by dividing the spectrometer response, adjusted to the wide slit setting, by the normalized sensitivity of Equation (IV-6).

Observations on Cascade Feeding and Resonance Self-absorption

The fact that visible light is emitted by the plasma is evidence that cascade feeding is a factor in the populating of some levels. Similarly, the presence of resonance self-absorption in He I during the calibration suggests that the noble gas neon will be subject to this effect too. We consider now just how severe an influence these phenomena will have on the theoretical models.

The effort to alleviate the cascade feeding in neutral neon has already been outlined. Their upper levels being only 1 eV below the continuum, Ne I 600 and Ne I 602 can be fed only by infrared transitions. For neon ions the energy levels of interest which are vulnerable to cascading are generally fed by UV transitions (Figures 5, 6, 7, 8). With the exception of the Ne II 1688 line to which the detector is insensitive, and the Ne V lines which were simply too weak for detection, these feed lines could be measured by the grazing incidence spectrometer.

One doubly ionized neon line subject to cascading is Ne III 313 which is fed by the Ne III 1256 multiplet (Figure 6). This multiplet should have appeared between the second order occurrence of Ne I 626 at 1252 Å and Ne I 629 at 1258 Å. Though it is still within the detector's capability to see, it was not seen--implying little if any cascading. The singlet states as well as the Ne III 489 multiplet (as mentioned before) have no known feeder lines.

Table 7. Relevant Neon Transitions with Wavelengths, Excitation Energies, Transition Probabilities, Oscillator Strengths, and Relative Intensities

Transition	λ (Å)	E_x (eV)	A_{ik} (10^8 sec ⁻¹)	f	Relative Intensity	$\frac{\Sigma A}{A_{ik}}$
$\Delta J = 1$	Ne I 602.7	20.56	.26	.0057	615	1.47
$\Delta J = 1$	Ne I 600.0	20.66	.35	.0042	478	1.67
$^2P_{\frac{1}{2}}^0 - ^2S_{\frac{1}{2}}^0$	Ne II 462.4	26.91	100	.33	8210	3.10
$^2P_{\frac{3}{2}}^0 - ^2S_{\frac{1}{2}}^0$	Ne II 460.7	26.91	210	.33	16500	1.48
$^3P_1 - ^3P_0^0$	Ne III 488.9	25.44	71	.085	300	1.00
$^3P_2 - ^3P_1^0$	Ne III 488.1	25.40	30	.063	353	2.37
$^1S_0 - ^1P_1^0$	Ne III 427.8	35.89	16	.13	31.1	14.1
$^1D_2 - ^1P_1^0$	Ne III 379.3	35.89	210	.27	797	1.07
$^3P_2 - ^3S_1^0$	Ne III 313.0	39.60	46	.041	58.6	1.76
$^1S_0 - ^1P_1^0$	Ne III 308.6	47.09	32	.14	43.8	2.41
$^1D_2 - ^1D_2^0$	Ne III 301.1	44.38	71	.097	118	1.00
$^3P_2 - ^3D_3^0$	Ne III 283.2	43.78	28	.047	66.2*	1.00
$^1D_2 - ^1P_1^0$	Ne III 282.5	47.09	45	.032	23.1	1.71
$^3P_2 - ^3P_2^0$	Ne III 267.1	46.42	23	.025	25.8*	1.35
$^3P_2 - ^3D_3^0$	Ne III 251.1	49.37	140	.18	17.3*	1.00
$^2D^0 - ^2D$	Ne IV 469.8	31.47	51	.17	64.1	1.15
$^2D^0 - ^2P$	Ne IV 358.7	39.64	150	.18	28.8	1.64
$^3P_3 - ^3D_2^0$	Ne V 572.3	21.80	14	.094	2.89	1.00
$^1D_2 - ^1D_2^0$	Ne V 416.2	33.54	110	.28	1.72	1.00

*These lines have components of intensity taken from multiplet structure.

For triply ionized neon, doublets are chosen because they apparently have less feeding potential (Figure 7). The Ne IV 607 line is not seen, and the Ne IV 432 doublet amounts to less than 10% of the intensity of Ne IV 470. The latter was easily corrected for this contribution.

This trend is assumed to hold up for Ne V and for Ne II for which no measurements were available. The neglect of cascade feeding thus seems to be quite reasonable.

The amount of resonance self-absorption determines whether the plasma is optically thin. Note that in the corona model, self-absorption is not a problem for any but resonance lines because only the ground state is significantly populated. Two tests for self-absorption are: (1) a variation of pressure¹⁰³ measuring the change of the quantity R_{uv}/R_{vis} as in the calibration experiment, Section IV, C, and (2) a comparison of theoretical and experimental intensities of multiplet components.¹⁰⁴ The former was not done because no visible spectrometer was mounted on ELMO. The latter has been done, and the close agreement (see Table 6 for the Ne III 489 multiplet and Table 7 for the Ne II 461 doublet which has a theoretical ratio of intensities of 2:1) indicates that the plasma is optically thin at least for ionic states. Because Ne I does not obey LS coupling,¹⁰⁵ the multiplet test was not possible for it. Judging from the experience with He I and He II, one might guess that for Ne I the system is less transparent. However, the difference between Ne I and Ne II, for which the plasma is optically thin, is only a factor of ten (for the optical path) times the density ratio, n_0/n_1 . If this ratio is about equal to one, then the degree of absorption for Ne I cannot be very great. In addition, self-absorption, which tends to reduce the observed

intensities, is partially canceled by cascade feeding which overfills the excited states according to the excitation model. The correct answer simply is not known. Therefore, let us proceed with the original assumption and the knowledge of what the potential error may be.

B. THE COLD-ELECTRON TEMPERATURE

Following the scheme of Section III, B, it is now possible to derive information not only about the cold-electron temperature, T_{ce} , but also the density ratio of the hot to cold-electron population, ϵ . Doubly ionized neon was the charge state chosen for this measurement. Ne I was passed over because of the uncertainty surrounding cascading and self-absorption; Ne II was not suitable because of the lack of appropriate atomic data. All eleven Ne III lines in Table 7 are employed.

The Hot to Cold-Electron Density Ratio

The ratios of theoretical excitation rates, R , may be calculated by Equation (III-22) and Equation (III-11) for any line pair or any value of ϵ . (Arithmetic and the numerical integration for this work were performed on a Digital Equipment Corporation PDP-12 computer using a variation of the FOCAL language.) Shown in Figure 13 is R versus T_{ce} for the line pair Ne III 488.1 and Ne III 379.3 for a family of ϵ 's. When matched with the experimental value of R from Equation (III-22), these curves imply an upper limit on the magnitude of ϵ , about 0.07 in this case. Additionally, although there is only a weak dependence on ϵ , the graphical solution for T_{ce} gives larger values as ϵ is reduced. The conclusion reached after study of several line pairs is that ϵ does not exceed 0.1. Incidentally, were the hot-electron temperature reduced, the limit on ϵ

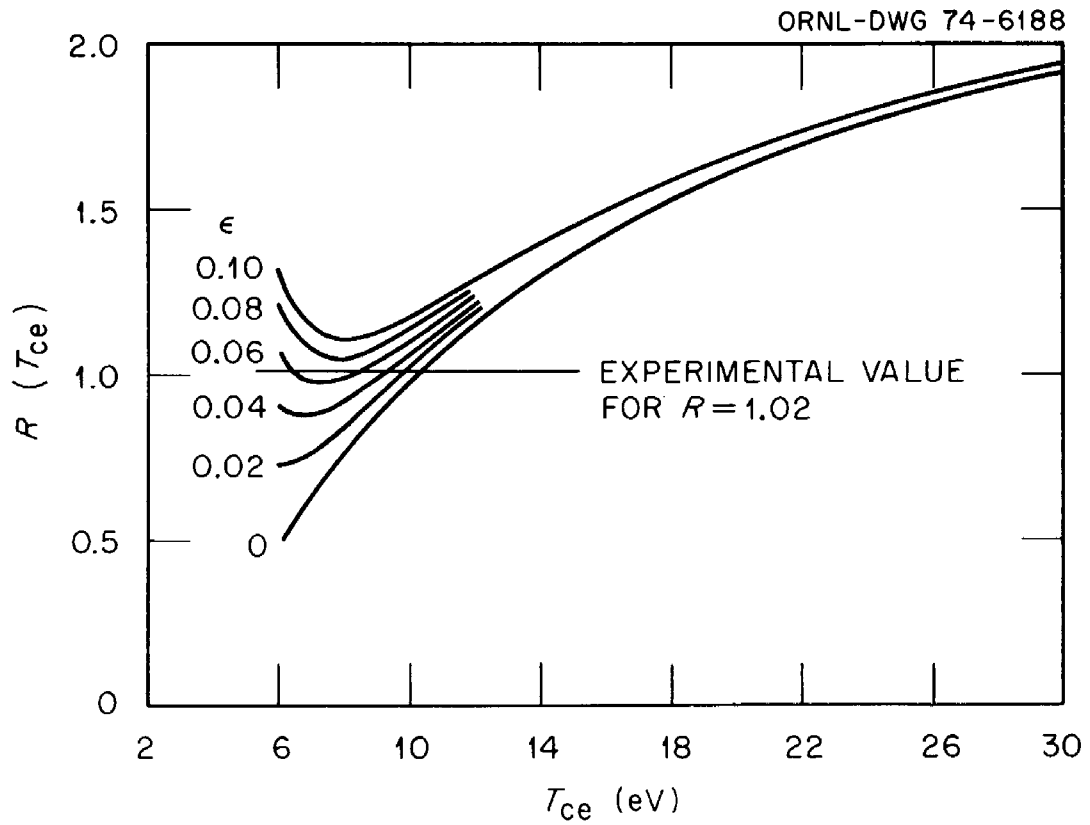


Figure 13. Theoretical Ratios of Excitation Rates of Ne III 379.3 and Ne III 488.1 for a Family of ϵ 's.

would become smaller. Information concerning a lower limit for ϵ will come out of the containment time calculation in Section V, D.

Determination of the Cold-Electron Temperature¹⁰⁶

It is established that the hot-electron component plays only a small role in the excitation process. Therefore, little error accrues if ϵ is set equal to zero and the hot electrons ignored. For this assumption, the solution in Figure 13 indicates that $T_{ce} \sim 10$ eV. Table 8 is a collection of these temperatures for the 55 combinations of the Ne III lines.

Values involving Ne III 488.9 and Ne III 251.1 are seen to deviate strongly from the rest of the data; thus, these points are not considered acceptable. Similarly, other pairs for which no solution is found are not considered further. This leaves 30 pairs with an average $T_{ce} = 13$ eV and a standard deviation of 6.5 eV. The discrepancy involving the Ne III 283.2 and Ne III 282.5 lines may be rectified without major changes for the other pairs if there is a 10% reduction in the experimental R value. That is, an assumed cumulative error of 10%, when removed, brings the temperature from this line pair to within two standard deviations of the given T_{ce} .

C. DENSITIES OF PLASMA CHARGE STATES

The new-found value of the cold-electron temperature enables us to proceed with our search for plasma parameters. The densities of the various neon ions and that of electrons are considered next.

Table 8. Solutions for the Cold-Electron Temperature from the 55 Pairs of Ne III Lines (in eV)

	488	427	379	313	309	301	283	282	267	251
489	*	-	-	-	29	60	95	95	160	8
	488	11	10	13	10	12	12	14	14	6
		427	*	22	10	11	13	17	19	<6
			379	38	10	12	14	19	21	<6
				313	8	8	9	15	17	<6
					309	6	6	*	<6	<6
						301	<6	-	-	<6
							283	96	-	<6
								282	6	<6
									267	<6

* These pairs have the same dependence on T_{ce} for excitation; no solution is possible because all values of T_{ce} are valid solutions.

Ion Density Calculations

Using $T_{ce} = 13$ eV to determine the $S_x(C)$ of Equation (III-16), the relative ground-state densities of different ions may be calculated via Equation (III-23). Table 9 presents an array of this data utilizing the three strongest lines of Ne III with those of the other charge states. It is found again that ϵ is not a critical parameter (less than 10% effect in the range $0 \leq \epsilon \leq 0.1$). An intermediate value, $\epsilon = 0.06$ was chosen for this table.

Table 9. Relative Ground State Densities of Five Neon Charge States as Determined by Pairs of Spectral Lines

		Ionic Charge of Numerators									
		0		1		2		3		4	
		600	462	461	488	379	301	470	359	572	416
602	600	1.22	.44	.42	.063	.048	.042	.0041	.0058	.000092	.000073
0	600	.36	.34	.052	.040	.034	.0034	.0048	.000076	.000060	
	462		.96	.14	.11	.10	.009	.013	.00021	.00017	
	1		461	.15	.12	.10	.010	.014	.00022	.00017	
				488	.77	.66	.066	.093	.0015	.0012	
					379	.86	.086	.121	.0019	.0015	
						301	.099	.139	.0022	.0018	
							470	1.40	.022	.018	
								359	.016	.013	
									572	.80	
											4

8

The values of n_k/n_0 for $k \neq 0$ are averaged over the appropriate points in the array, and from this and Equation (III-26), the fractional populations are figured. Placing the numbers 300°K and 2.5×10^{-6} Torr into Equation (III-27) for the temperature and pressure, one finds the total particle density to be $n_T = 8.0 \times 10^{11} \text{ cm}^{-3}$. Hence, as in Table 10, the absolute ion densities are determined.

Table 10. Fractional Populations and Densities of Neon Charge States for $n_T = 8.0 \times 10^{11} \text{ cm}^{-3}$

Ionic Charge, k	Fractional Population, F_k	$n_k \text{ (cm}^{-3}\text{)}$
0	.69	5.6×10^{11}
1	.27	2.2×10^{11}
2	.033	2.6×10^{10}
3	.0031	2.5×10^9
4	.00005	4.2×10^7

Electron Density Calculations

Immediately, from Table 10 and Equation (III-28), it is discovered that the total electron population must be $n_e = 2.8 \times 10^{11} \text{ cm}^{-3}$. Then, the approximate densities of hot and cold electrons come from Equation (III-29). Assuming $\epsilon = 0.06$, we have $n_H \sim 1.6 \times 10^{10} \text{ cm}^{-3}$ and $n_C \sim 2.6 \times 10^{11} \text{ cm}^{-3}$.

D. DETERMINATION OF CONTAINMENT TIME AND ION TEMPERATURE

Now that there is something to which one may compare the solutions of the theoretical ion population equations, the particle containment time, τ_c , and the ion temperature, T_i , may be evaluated.

Particle Containment

Equation (I-2) is now used to convert electron temperatures to energies. This having been done, the ionization rates for the cold electrons ($E = 19.5$ eV) are interpolated from Lotz's tables¹⁰⁷ using Aitken's method¹⁰⁸ for a cubic polynomial fit. As stipulated, the rates for the hot component ($E = 30$ keV) are calculated.

The solutions of Equation (III-44) and Equation (III-46) may now be computed by the PDP-12. Figure 14 shows the time evolution of the F_k 's thus obtained from the theoretical ionization model for $\epsilon = 0.06$. Table 11 displays a portion of the computer output for the time interval of interest. The experimental value of F_0 is found in the Ne I column of this table. The corresponding time, 180 microseconds in this case, is taken as τ_c . Ideally, the experimental F_k 's could be read straight across the table for this time. How well the theoretical values fit the numbers of Table 10 is a test of the worth of the ionization model employed. Table 12 gives the ratios of such values to the experimental F_k 's for several ϵ 's.

Several points can be made from Table 12:

- (1) τ_c is about the same regardless of the hot-electron content of the plasma. We shall use 180 microseconds in a later calculation.

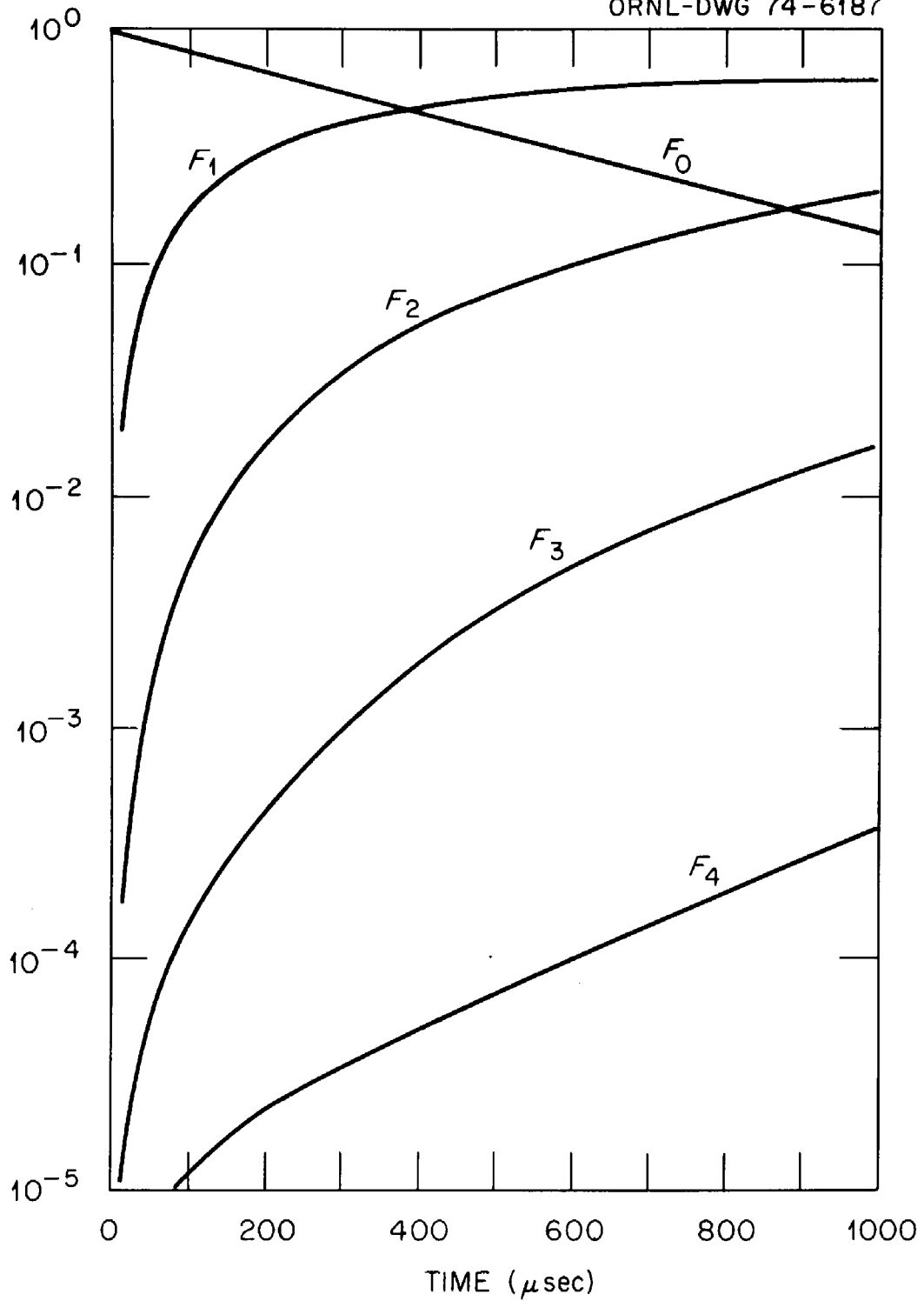


Figure 14. The Theoretical Time Evolution of the F_k 's for $\epsilon = 0.06$.

Table 11. A Computer Printout for the Time Dependence of the Fractional Populations of the Neon Charge States

	EL ECTRON TEMPERATURE	EL ECTRON DENSITY
COLD COMPONENT	13 EV	0.260377E+12
HOT COMPONENT	20 KEV	0.156226E+11

TIME IN MICROSECONDS E = .06

TIME	NE I	NE II	NE III	NE IV	NE V
150	0.742706	0.246238	0.010733	0.000257	0.000017
160	0.728123	0.259528	0.011992	0.000287	0.000019
170	0.713826	0.272472	0.013308	0.000319	0.000019
180	0.699810	0.285078	0.014680	0.000354	0.000021
190	0.686069	0.297351	0.016107	0.000391	0.000022
200	0.672598	0.309301	0.017586	0.000430	0.000023
210	0.659392	0.320931	0.019115	0.000472	0.000024
220	0.646445	0.332251	0.020695	0.000518	0.000025
230	0.633752	0.343266	0.022321	0.000565	0.000025
240	0.621308	0.353982	0.023994	0.000617	0.000028
250	0.609109	0.364405	0.025713	0.000671	0.000027
260	0.597149	0.374543	0.027474	0.000728	0.000029
270	0.585424	0.384400	0.029278	0.000788	0.000031
280	0.573929	0.393983	0.031122	0.000852	0.000032
290	0.562660	0.403298	0.033005	0.000920	0.000033
300	0.551612	0.412349	0.034928	0.000990	0.000034
310	0.540781	0.421143	0.036887	0.001065	0.000035
320	0.530163	0.429686	0.038881	0.001142	0.000037
330	0.519753	0.437981	0.040910	0.001224	0.000038
340	0.509548	0.446036	0.042972	0.001309	0.000041
350	0.499544	0.453853	0.045067	0.001399	0.000040
360	0.489735	0.461440	0.047192	0.001491	0.000044
370	0.480119	0.468801	0.049347	0.001588	0.000044
380	0.470692	0.475940	0.051531	0.001689	0.000047
390	0.461450	0.482861	0.053743	0.001794	0.000048
400	0.452389	0.489572	0.055980	0.001904	0.000050

Table 12. The Ratio of Theoretical to Experimental F_k 's*

ϵ	Ne I	Ne II	Ne III	Ne IV	Ne V	Time (microsec.)
.00	1.01	1.07	.30	.02	-	200
.02	1.00	1.10	.38	.05	.15	200
.06	1.01	1.05	.45	.11	.40	180
.06**	1.01	1.05	.39	.05	-	180
.10	1.01	1.05	.53	.17	.60	170

* The experimental numbers are all taken from the case $\epsilon = 0.06$; their dependence on ϵ is not strong.

** For this case, the multi-step ionization mode is not included.

(2) The fit of the data for Ne III, Ne IV, and Ne V improves as ϵ increases. We have used 0.1 as an upper limit; we may now say something about the lower limit. As noted before, excitation is dominated by the cold electrons; however, the higher charge states are very dependent on the hot component. Their presence spectroscopically is proof that a hot-electron population must be present also. A crude guess as to the minimum value of the hot-electron density is $n_H \sim 0.02 n_C$.

(3) Multi-step ionization of neutrals enhances the populations of the multi-charged ions. Doubly ionized particles are increased 15% by the turning on of the $\Delta k > 1$ mode for $\epsilon = 0.06$, and the triply charged neon population doubles. Ne V improves by over a factor of ten.

(4) The fit for Ne IV and Ne V would be better if multi-step ionization of Ne II were included--not so for Ne III because its formation from Ne II is a single-step ionization.

Ion Heating

The suggested containment time is found to be less than the mean lifetime before ionization of neutral particles trapped in the cavity [Equation (III-47)]. Obviously, there is very little heating of ions. For a maximum calculation, T_i may be determined from Equation (II-3) using $\Delta t = \tau_c$. The heating rate is approximately 60 eV/sec; therefore, the maximum energy gain an ion may be expected to achieve is 0.01 eV or about 130° Centigrade. The peak value then is $T_i \sim 0.04$ eV.

E. ERROR ANALYSIS

Included in this section on observations and measurements is a summary of sources of error in the outlined procedures. This is broken into two parts: experimental error and error from the various ideas and data out of which the theoretical models are constructed.

Experimental Errors

The crucial question of experimental errors deals with whether the response of the spectrometer-detector system as corrected is a true measure of the light intensity of a particular atomic transition. One of the largest factors in answering this inquiry is the intensity calibration. The calibration is essentially based on only three wavelengths, circa 240, 520, and 970 Å, from which a straight-line sensitivity function is assumed. While cascading is no problem in the calibration, self-absorption is not handled well so that a 20% error in the relative intensities is not hard to imagine. On the plus side, most of the wavelengths of interest reside in a relatively narrow wavelength interval over which the instrument sensitivity should be fairly flat.

Detector saturation is not expected to be a problem because of the manipulation of the slits. However, changing the slits introduces a new uncertainty--maybe 20%.

Another factor is the time variation of the plasma. The steady-state condition is only approximate. Thus, source parameters may change between measurements of different line intensities.

Finally, the absolute densities are very dependent on the ionization gauge measurements. As stated in Section II, a calibration was assumed for the ELMO gauge. Additionally, the assumption of a temperature for particles in the gauge influences the outcome of the density results.

Theoretical Errors

Many assumptions have been made in the formation of the theoretical models. Thus, the models contain many elements of inherent error.

For example, concerning light intensity, cascade feeding and resonance self-absorption have been ignored. These problems would appear most evident in the measurement of the neutral lines as has been suggested.

The neglect of secondary excitation modes, e.g., simultaneous ionization and excitation, has resulted in perhaps a 10% error as was commented earlier. Besides this are the assumptions related to the form of the excitation rates, $S_x(C)$ and $S_x(H)$. Neither function takes multiplicity into account for example. The Maxwellian nature of the cold-electron distribution (mentioned again at the end of this topic of discussion) and the delta function for the hot component have not been verified. In fact, the argument of the delta function for the hot

electrons (20 keV) is only a guess. Following Equation (III-18) it is suggested that by taking $T_H = 20$ keV, perhaps a 12% mistake is made in $S_x(H)$. In view of the fact that the hot electrons are unimportant to the excitation process, this is a second order problem however.

One large source of error involves the A_{ik} 's which may be correct only within a factor of two.¹⁰⁹ For instance, the line pairs Ne III 379-Ne III 427 and Ne III 308-Ne III 282.5, having in both cases the same upper state, should have the ratio of their intensities equal to the ratio of their transition probabilities according to Equation (III-20). This is found not to be the case (Table 7), implying that one or both of the A_{ik} 's is incorrect for both pairs. This will make a difference for both the excitation and the ionization models.

Similarly, the presence of metastables is an unmeasured quantity which alters both models. Koozekanani¹¹⁰ has pointed out that in neon, a metastable neutral has a higher ionization cross section than a ground-state neutral. This effect does not disturb ionic populations because only for neutrals is the metastable level close to the ionization level of the atomic system. In a like sense, excitation from a metastable must be easier than excitation from the ground state simply because the metastable electron is less tightly bound to the nucleus.

Nonresonant neutral charge exchange, as was stated, is a small effect for doubly ionized neon. No information, however, is available concerning higher states of ionization. Such a phenomenon would tend to reduce the populations of higher charge states and neutrals in favor of singly and doubly charged neon. Nevertheless, this is suspected to be a very small factor.

A larger cause for concern might be the ionization cross sections herein applied. Lotz¹¹¹ estimates the error in his ionization rate data as +40% to -30%. The second order effect of errors in the multi-step ionization cross sections is reflected by the cross section data of Schram and others¹¹² which is only a third the magnitude of the data used for Section V.

Yet another small effect is ionic recombination. The insignificance of this may now be demonstrated however. Using $T_{ce} = 13$ eV in Equation (III-10), we have for $k = 4$, $\alpha \sim 1.1 \times 10^{-12}$ cm³/sec. At this temperature, the $S_x(C)$'s which pertain to Ne V 572 and Ne V 416 are given by Equation (III-16) as 7×10^{-10} and 5×10^{-10} cm³/sec. Thus, four-times-ionized atoms are several hundreds of times more likely to be excited by than to recombine with the background electrons. Because of the charge dependence of α , lower charge states are even less affected.

Finally, consider two other assumptions. One is the complete neglect of the energetic electron annulus. This is not so bad because first, the number of particles so neglected is relatively small, and secondly, the rate coefficients for ionization and excitation decrease with energy. We have already seen the ineffectiveness of the 20 keV electrons in the excitation process. Last is the assumption of a uniform plasma. It could be that both temperature and density are space dependent contrary to the assumptions which were made. Yet Equation (I-11) suggests that the equilibrium time for the cold electrons is very short--implying that they exist in at least a quasi-Maxwellian equilibrium.

The Effect on Calculated Parameters

The least disturbed intrinsic parameter measurement is for T_{ce} . This was done on Ne III so that none of the neutral problems enter into play. The spread on the data using the standard deviation is $\pm 50\%$, but this is really rather good because T_{ce} is so low. The measurement puts a firm upper bound on the cold-electron temperature.

Relative ground-state densities are seen to vary by as much as a factor of two between line pairs of the same two charge states. Another indication of the cumulative error is found in the boxes of Table 9 for which both lines in a pair correspond to the same charge state. These numbers should equal one. A factor of two is a reasonable maximum error to be expected for this measurement. The same holds true for ϵ , the ratio of hot to cold electron densities.

Absolute density measurements must include another set of uncertainties; hence, an additional factor-of-two error is possible.

The incompleteness of the ionization model accounts for its lack of decisiveness without even worrying about errors. Particle losses, etc., negate confidence that T_i and τ_c are correct within a factor of two or three. Note that T_i could not be a factor of two lower since room temperature represents a minimum at 0.026 eV. Also, notice that $\tau_c = 180$ microseconds is about half the time necessary for room-temperature particle to cross the cavity (Section II, B). Were τ_c determined by F_2 or F_4 , it would be 290 or 400 microseconds respectively--even more if F_3 were used.

VI. CONCLUSION

This final section contains a comparison of the plasma parameters measured during this experiment with those of previous workers. Following this is a critical summary of the success of the theoretical model used with possible applications and suggestions for future work.

A. COMPARISON OF MEASUREMENTS

Intrinsic plasma parameters which may be compared are as follows:

Electron Parameters

We found in Section II that usually $n_e \sim 10^{12} \text{ cm}^{-3}$. This compares to $n_e \sim 2.8 \times 10^{11} \text{ cm}^{-3}$ as measured in this thesis. As expected, the contribution of hot electrons is less than that of the cold ones to the overall electron density. That ϵ is perhaps smaller in this experiment may be a manifestation of the higher atomic weight of neon.

This was the first explicit measurement of the cold-electron temperature. We may compare $T_{ce} = 13 \text{ eV}$ with the estimate, cited in Section II, of tens of electron volts.

Ion Parameters

Particle energy and containment times agree qualitatively with past experience. The ions are not contained and are not heated. This experiment also agrees with others that several ionic states coexist within the plasma.

B. THE SUCCESS OF THE THEORETICAL MODEL

The success of the physical models used for this dissertation is that in principle many intrinsic plasma parameters may be derived spectroscopically. Not only this, but also these models yield qualitative agreement with previous studies done on ELMO plasmas. These quantities have been determined with a probable doubt of no more than a factor of two. Included among them are the temperature of the cold-electron background plasma, the ion temperature, the densities of the several charge states, and the electron density. Moreover, a particle containment time has been found as well as a division of the electron population into a hot and cold group.

Some special features should be emphasized. The first is that a hot-electron component is necessarily included in the ionization model to account for the spectroscopic observations. The second point is that multi-step ionization does play a significant role in the sustenance of the highly charged ion populations within ELMO. Thus, we have seen the importance of the hot electrons in the ELMO plasma re the ionization processes. Finally, we have learned that the atomic excitation mechanism unlike the ionization process, does not depend on the energetic plasma components. Rather, it is the cool background electrons which are of paramount importance here.

C. POSSIBLE APPLICATIONS

There is a sizable number of applications for the ideas incorporated in this dissertation. Some of these are listed below.

High-Z Ion Sources

Several authors^{113,114} have proposed ELMO as a source of highly stripped heavy ions. Presumably, highly charged ions of krypton, xenon, etc., would be present as were those of neon and argon. Knowing the wavelengths of the ions' radiative transitions, one could determine the densities of the charge states and estimate the flux of particles through a small hole in the end of the machine. Assuming no preferred direction of motion among the ions, the current density, J , is given by the elementary law of kinetic theory:

$$J = \frac{n q v}{4} \quad . \quad (VI-1)$$

For the present experiment, Ne^{4+} with $v \sim 6 \times 10^4$ cm/sec and $n_4 \sim 4 \times 10^7$ cm⁻³ yields 4×10^{-7} amperes/cm².

Impurity Radiation

Bremsstrahlung radiation arises in plasmas at the expense of electron and ion temperature; hence, it is an important loss mechanism in plasmas of thermonuclear interest. Because the energy loss rate is proportional to the square of the ionic charge, the presence of highly charged impurity ions in the plasma is very serious.¹¹⁵

A possible application of the techniques of this paper is the determination of bremsstrahlung losses from impurity ions. The

ground-state populations of the highly charged ions in a quasi-steady-state system could be measured with careful modifications of Equation (III-21), etc. Then the radiation losses could be accurately judged. By "quasi-steady-state system" is meant an experiment in which plasma parameters change slowly compared to the time for the measurements of spectral signals. An important alteration in the excitation model would be the inclusion of atom-atom collisions since the ion temperature would be quite high.

Excitation and Ionization Rates

In this research, certain plasma parameters have been derived using coefficients measured by Hinnov.¹¹⁶ He did his work by the reverse process. Knowing well the temperature and densities in his plasma, he calculated the excitation and ionization rates of neon. One may follow the same tactics to discover such information about other elements. Also, the ionization rates for multi-step ionization could be estimated.

D. SUGGESTIONS FOR FUTURE WORK

Certain corroborating experiments would have been helpful in the present research. A bremsstrahlung spectra from which one investigates the hot electrons' temperature and density has not been reported using neon or any other high-Z gas. Whether or not the characteristics of the electron populations change is an open question. For another instance, Dandl has suggested¹¹⁷ the use of a gridded probe to confirm the cold-electron temperature.

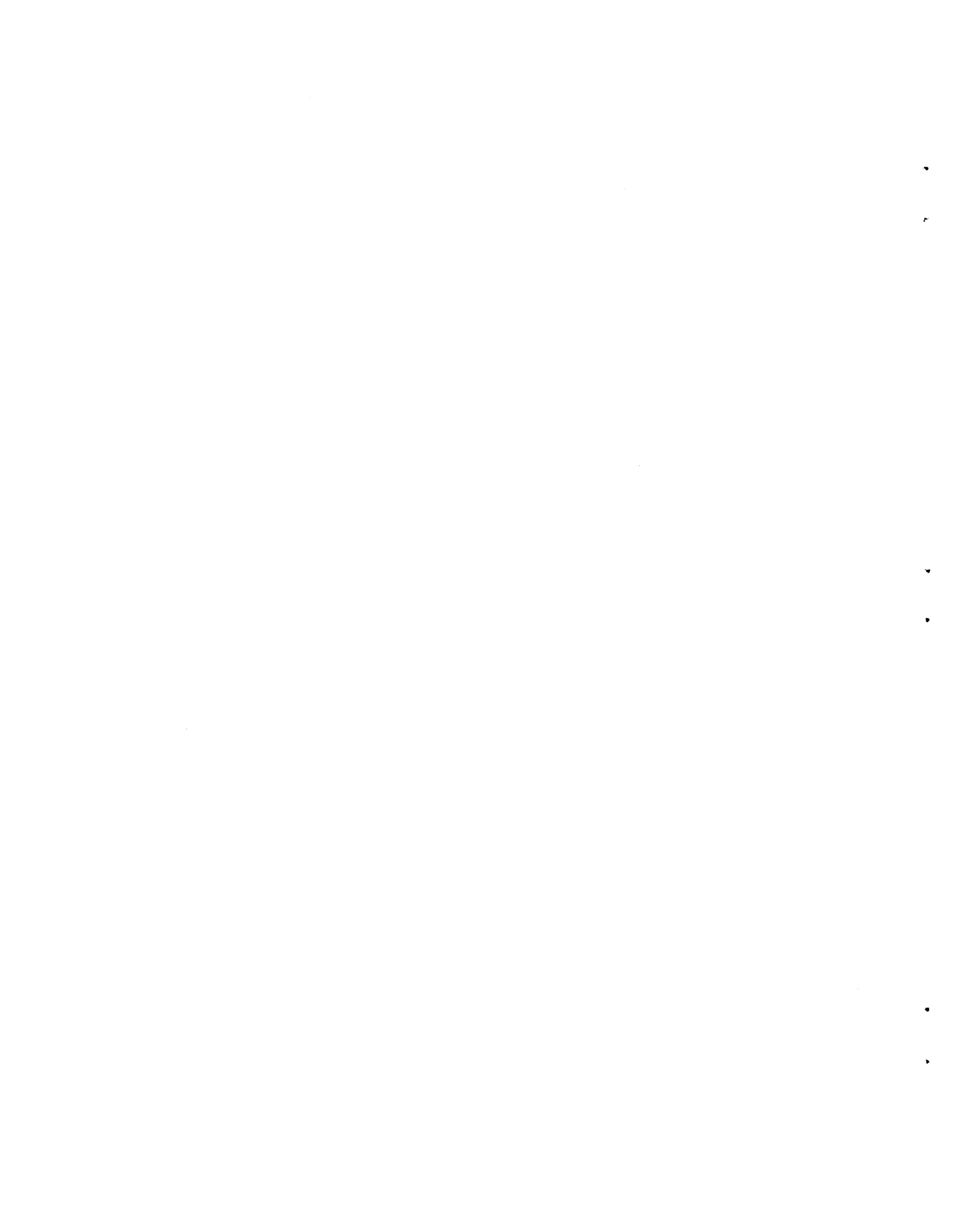
Preliminary data were taken using argon before the shutdown. The worth of ELMO as an ion source of Ar^{7+} , Ar^{8+} , etc., has yet to be

quantitatively appraised. Such a project would be of use to nuclear physicists.

Unfortunately, spectroscopic examination of krypton or xenon would be difficult because atomic data for the higher ionization states, including their spectra, are unknown. However, the spectra of these gases in ELMO would contain information about these ions from which energy levels and other atomic data could be inferred. A person interested in the atomic structure of Xe^{8+} , Xe^{9+} , Xe^{10+} , and so on, would have a steady-state source of the line radiation from these species with which he could work.

A very interesting problem is the multi-step ionization of ions. By including losses in the models--perhaps by measuring the flux of different ions from the mirror trap--the methods described in this paper might be used to estimate the $\Delta k > 1$ rates. Given control over the distribution function of hot electrons, say by pressure and microwave power regulation, the actual cross sections could be guessed.

Finally, the techniques of this thesis are recommended for assessing the effect of impurities in fusion-oriented machines. As stated, this application is possible whenever the measurements are fast compared to the rate of change of the plasma parameters. Thus, even a pulsed device with a plasma lifetime on the order of milliseconds could be so diagnosed.



LIST OF REFERENCES

1. F. I. Boley, Plasmas--Laboratory and Cosmic (D. van Nostrand Co., Inc., Princeton, N. J., 1966), p. 13.
2. S. G. Glasstone and R. H. Lovberg, Controlled Thermonuclear Reactions (Van Nostrand Reinhold Co., New York, 1960) p. 84.
3. L. Spitzer, Physics of Fully Ionized Gases (Interscience Publishers, New York, 1962), p. 21.
4. Reference 3, p. 22.
5. Reference 2, p. 85.
6. Reference 2, p. 85.
7. D. J. Rose and M. C. Clark, Plasmas and Controlled Fusion (M.I.T. Press, John Wiley & Sons, Inc., New York, 1961), p. 184.
8. Reference 1, p. 51.
9. W. C. Gough and B. J. Eastlund, Scientific American 224, 50 (Feb. 1971).
10. C. L. Longmire, Elementary Plasma Physics (Interscience Publishers, New York, 1967), p. 25.
11. J. R. Reitz and F. J. Milford, Foundations of Electromagnetic Theory (Addison-Wesley Publishing Co., Reading, Mass., 1967), p. 272.
12. Reference 9.
13. W. T. Scott, The Physics of Electricity and Magnetism (John Wiley and Sons, Inc., New York, 1959), pp. 281, 294.
14. J. Thewlis, Encyclopaedic Dictionary of Physics (Pergamon Press, New York, 1961), Vol. 3, p. 677.
15. Reference 3, p. 9.
16. A. Simon, An Introduction to Thermonuclear Research (Pergamon Press, New York, 1959), p. 86.
17. Reference 2, pp. 93, 96.
18. M. S. Ioffe, Plasma Physics (IAEA, Vienna, 1965), p. 424.
19. Reference 18, pp. 424, 425.

20. G. E. Guest, Theory of High-Frequency Instabilities in Mirror-Confined Plasmas, Oak Ridge National Laboratory, Oak Ridge, Tenn., Rept. ORNL-TM-2864 (1970).
21. F. R. Scott, T. H. Jensen, and C. B. Wharton, Plasma Physics and Controlled Nuclear Fusion Research (IAEA, Vienna, 1966), Vol. II, p. 463.
22. L. A. Ferrari and A. F. Kuckes, Phys. Fluids 8, 2295 (1965).
23. C. W. Hartman, Phys. Fluids 9, 821 (1966).
24. W. B. Ard, R. A. Dandl, and R. F. Stetson, Phys. Fluids 9, 1498 (1966).
25. G. E. Guest and D. J. Sigmar, Nucl. Fusion 11, 151 (1971).
26. R. A. Dandl *et al.*, Plasma Physics and Controlled Nuclear Fusion Research (IAEA, Vienna, 1968), Vol. II, p. 435.
27. R. A. Dandl *et al.*, Plasma Physics and Controlled Nuclear Fusion Research, (IAEA, Vienna, 1971), Vol. II, p. 607.
28. O. C. Eldridge, Phys. Fluids 15, 676 (1972).
29. A. van der Woude, IEEE Trans. Nucl. Sci. NS-19, No. 2 (1972).
30. R. A. Dandl (unpublished, April 1973).
31. G. R. Harrison *et al.*, Practical Spectroscopy (Prentice-Hall, Inc., New York, 1948) pp. 11, 20.
32. J. Richter, "Radiation of Hot Gases," in Plasma Diagnostics, ed. by W. Lochte-Holtgreven (North-Holland Publishing Co., Amsterdam, 1968), p. 3.
33. W. Lochte-Holtgreven, "Evaluation of Plasma Parameters," in Reference 32, p. 184.
34. R. Linke, "Vacuum Ultraviolet Spectroscopy," in Reference 32, p. 347.
35. R. W. P. McWhirter, "Spectral Intensities," in Plasma Diagnostic Techniques, ed. by R. H. Huddlestone and S. L. Leonard (Academic Press, New York, 1965), p. 201.
36. J. H. Leck, Pressure Measurements in Vacuum Systems (Chapman and Hall, Ltd., London, 1964), p. 92.
37. S. Dushman and A. H. Young, Phys. Rev. 68, 278 (1945).
38. H. Ikegami *et al.*, Phys. Rev. Letters 19, 778 (1967).

39. N. I. Vinogradov *et al.*, *Sov. Phys.-Tech. Phys.* 16, 739 (1971).
40. R. A. Dandl *et al.*, Relativistic Plasmas: The Coral Gables Conference (W. A. Benjamin, Inc., New York, 1968), p. 181.
41. P. H. Edmonds *et al.*, *Bull. Am. Phys. Soc.* 13, 1490 (1968).
42. Reference 27.
43. R. A. Dandl *et al.*, *Nucl. Fusion* 11, 411 (1971).
44. Thermonuclear Div. Semiann. Progr. Rept. Oct. 31, 1965, ORNL-3908, p. 43.
45. Thermonuclear Div. Semiann. Progr. Rept. April 30, 1963, ORNL-3472, pp. 27, 29.
46. Reference 40.
47. Reference 27.
48. Reference 44.
49. Reference 40.
50. Reference 27.
51. G. E. Guest, Comments on Plasma Physics and Controlled Fusion (Comments in *Modern Physics: Part E*) 1, 29 (1972).
52. Reference 2, p. 98.
53. H. Postma, *Phys. Letters* 31A, 196 (1970).
54. Reference 29.
55. Reference 30.
56. C. W. Allen, Astrophysical Quantities (Athlone Press, London, 1955), p. 42.
57. Reference 32, p. 45.
58. H. R. Griem, *Phys. Rev.* 131, 1170 (1963).
59. Reference 35, pp. 208, 209.
60. Reference 35, p. 222.
61. L. G. Christophorou, Atomic and Molecular Radiation Physics (Wiley Interscience, New York, 1971), p. 95.

62. J. B. Hasted and M. Hussain, Proc. Phys. Soc. 83, 911 (1964).
63. W. E. Lamb and M. Skinner, Phys. Rev. 78, 539 (1950).
64. S. H. Koozekanani, Phys. Rev. 176, 160 (1968).
65. Reference 35, p. 211.
66. E. Hinnov, J. Opt. Soc. Amer. 56, 1179 (1966).
67. Reference 33, pp. 186, 187.
68. W. Lotz, Astrophys. J. Suppl. 14, 237 (1967).
69. W. Lotz, Zeitschrift P. 216, 241 (1968).
70. W. Lotz, J. Opt. Soc. Amer. 58, 915 (1968).
71. F. A. Stuber, J. Chem. Phys. 42, 2639 (1965).
72. Reference 61, p. 126.
73. E. H. S. Burhop, The Auger Effect and Other Radiationless Transitions (Cambridge, London, 1952), p. 2.
74. T. A. Carlson and M. O. Krause, Phys. Rev. 140, A1057 (1965).
75. Reference 70.
76. T. A. Carlson *et al.*, Phys. Rev. 169, 27 (1968).
77. T. A. Carlson and C. W. Nestor, Phys. Rev. A 8, 2887 (1973).
78. T. A. Carlson, Phys. Rev. 156, 142 (1967).
79. A. Migdal, J. Phys. (U.S.S.R.) 4, 449 (1941).
80. T. A. Carlson, Phys. Rev. 130, 2361 (1963).
81. T. A. Carlson *et al.*, Phys. Rev. 151, 41 (1966).
82. M. J. van der Wiel *et al.*, Physica 42, 411 (1969).
83. J. A. R. Samson, Techniques of Vacuum Ultraviolet Spectroscopy (John Wiley and Sons, Inc., New York, 1967), p. 5.
84. Instruction Manual: Operating Instructions for Model 247 Grazing Incidence Monochromator Spectrograph (McPherson Instrument Corp., Acton, Mass.), 1.1.
85. Reference 83, p. 5.

86. Reference 84, 7.1b.
87. Reference 31, pp. 28, 34, or any standard optics text.
88. Reference 84, grating information.
89. Reference 83, p. 35.
90. Reference 84, 2.1.
91. Mullard Channel Electron Multipliers (Mullard Limited, London, 1967), p. 1.
92. J. A. Ray and C. F. Barnett, IEEE Trans. Nucl. Sci. NS-17, No. 1, 44 (1970).
93. C. S. Weller and J. M. Young, Applied Optics 9, 505 (1970).
94. A. R. Striganov and N. S. Sventitskii, Tables of Spectral Lines of Neutral and Ionized Atoms (IFI/Plenum, New York, 1968).
95. R. L. Kelly, Atomic Emission Lines Below 2000 Angstroms-Hydrogen Through Argon, NRL-6648 (1968).
96. E. Hinnov and F. W. Hofmann, J. Opt. Soc. Amer. 53, 1259 (1963).
97. W. B. Ard *et al.*, Plasma Physics and Controlled Nuclear Fusion Research (IAEA, Vienna, 1971) Vol. II, p. 619.
98. Reference 94, p. 224.
99. Reference 56, pp. 54, 55.
100. W. L. Wiese *et al.*, Atomic Transition Probabilities - Hydrogen Through Neon, NSRDS-NBS4, Vol. 1 (1966).
101. G. M. Lawrence and H. S. Liszt, Phys. Rev. 178, 122 (1969).
102. Reference 100, pp. x, xi.
103. N. H. Lazar and E. Hinnov, private communications.
104. Reference 33, pp. 136, 137.
105. G. Racah, Phys. Rev. 61, 537 (1942).
106. J. A. Cobble, to be published in Applied Optics.
107. Reference 68.
108. M. Abramowitz and I. S. Stegun, eds., Handbook of Mathematical Functions, National Bureau of Standards, Applied Mathematics Series 55, 879 (1964).

109. Reference 100.
110. Reference 64.
111. Reference 68, p. 231.
112. B. L. Schram *et al.*, *Physica* 32, 185 (1966).
113. Reference 53.
114. A. Zucker, Conf. on Heavy Ion Sources, Washington, D.C., March 13, 1970 (WASH-1159), p. 141.
115. Reference 7, pp. 234, 235.
116. Reference 66.
117. R. A. Dandl, private communication.